

## "Context-dependent evolutionary dynamics toward bacterial survival during sequential antibiotic treatment"

Adam Lyon<sup>1</sup>, Muhammed Sadik Yildiz<sup>1</sup>, Samuel Cooke<sup>2</sup>, Adam Rosenthal<sup>2</sup>, Erdal Toprak<sup>1,3,4</sup>

<sup>1</sup> Department of Pharmacology, The University of Texas Southwestern Medical Center, Dallas, TX 75390, USA

<sup>2</sup> Department of Microbiology and Immunology, University of North Carolina, Chapel Hill, NC, USA

<sup>3</sup> Lyda Hill Department of Bioinformatics, The University of Texas Southwestern Medical Center, Dallas, TX 75390, USA

<sup>4</sup> Lead contact (Erdal.Toprak@utsouthwestern.edu)

### ABSTRACT

Solving the antibiotic resistance problem necessitates optimizing antibiotic use through evolutionary insights. Laboratory evolution studies commonly reveal cross-resistance and collateral sensitivity phenotypes, but how these phenotypes influence clinical success in sequential antibiotic therapies remains unclear. We developed a new laboratory evolution protocol that partially simulates clinical antibiotic pharmacodynamics by applying strong selection pressure while preserving population diversity. Using this method, we evolved *Escherichia coli* under single or sequential antibiotic exposures until sustained survival emerged. Although the final phenotypes appeared similar, distinct and reproducible evolutionary trajectories were evident, characterized by antibiotic-specific mechanisms of resistance, persistence, and tolerance. Remarkably, sequential antibiotic use prompted evolutionary shifts from genetically divergent to convergent trajectories, highlighting strategies to refine antibiotic use, enhance clinical efficacy, and mitigate the risk of multi-drug resistance. Single-cell RNA sequencing further revealed distinct and shared gene expression dynamics linked to mutation profiles in evolved cultures. These evolutionary insights have the potential to inform and improve antibiotic treatment strategies, warranting further investigation.

## **INTRODUCTION**

Antibiotic resistance is a global health crisis causing over one million deaths annually and projected to result in 2-10 million deaths per year by 2050<sup>1,2</sup>. With limited new antibiotics in development, optimizing evidence-based antibiotic choices is essential to prolong the efficacy of current and future antibiotic compounds. Repeated treatment failures can lead to multi-drug resistant (MDR) infections, which are associated with higher morbidity and mortality<sup>3</sup>. Therefore, antibiotic choices must consider both clinical efficacy and the evolutionary consequences of treatment failures to mitigate these risks. Beyond resistance, treatments may fail due to non-canonical bacterial survival strategies, including persistence, tolerance, and evasion of antibiotic exposure within parts of the body<sup>4,5</sup>. Studies have highlighted the importance of evolutionary dynamics in resistance between antibiotic pairs<sup>6</sup>. For instance, antibiotic pairs should be avoided where resistance to one antibiotic confers cross-resistance to another<sup>7-9</sup>. Rather, pairs which induce collateral sensitivity or orthogonal resistance mechanisms should be prioritized to ensure immediate and long-term clinical success<sup>10,11</sup>. However, the impact of evolutionary dynamics on regimens requiring multiple antibiotics and the full spectrum of bacterial survival strategies remains mostly uncharted. To address this gap, we employed a laboratory evolution protocol that better simulates antibiotic pharmacodynamics in clinical treatments by using strong selection while maintaining population diversity. Using this protocol, we evolved *Escherichia coli* populations with single or multiple, sequential antibiotics until they achieved sustained survival. Although the phenotypic outcomes were similar, evolutions using single antibiotics or multiple sequential antibiotics produced distinct and reproducible differences among the associated mutational trajectories. We found that bacteria employ diverse resistance, persistence, and tolerance mechanisms, specific to each antibiotic, to evade strong killing effects induced by antibiotics. Most strikingly, we observed transitions from divergent to convergent evolutionary patterns when antibiotics were used sequentially, which we hypothesize could be leveraged to improve antibiotic choice, enhance clinical efficacy, and mitigate MDR development. Despite the high frequency of the mutations, by employing single-cell RNA sequencing of evolved bacterial cultures, we observed diverse gene expression dynamics in clusters of single cells. These subpopulations too could be the target of rational treatment design.

## **RESULTS**

### **Distinct survival trajectories emerge during bacterial adaptation to high-dose antibiotic treatments in a clinically relevant evolution model.**

We quantitatively evaluated the evolutionary consequences and trade-offs associated with antibiotic treatment failures for single compounds. We evolved ten replicate isogenic cultures of a laboratory strain of *E. coli* (K-12, MG1655, abbreviated here as MG) to one of three antibiotics, levofloxacin, amikacin, or cefepime (30 cultures in total). Each antibiotic represents a separate antibiotic class and mechanism of action, and they were chosen due to their frequent empirical and prophylactic use in clinics, particularly in pediatric stem cell transplant patients. Levofloxacin is a fluoroquinolone that targets DNA synthesis through DNA gyrase inhibition<sup>12</sup>. Amikacin is an aminoglycoside that binds the 30s ribosomal subunit causing mistranslation and in turn killing bacteria through proteotoxic stress<sup>13,14</sup>. Cefepime is a cephalosporin, a beta lactam antibiotic, that disrupts a key step in cell wall synthesis<sup>15</sup>. In addition, four untreated isogenic MG cultures were passaged daily without any antibiotic exposure as a control.

Our evolution protocol was designed to reveal clinically relevant bacterial survival strategies and associated genetic changes. In clinical settings, antibiotic concentrations routinely peak and trough in human body, consistently remaining above the minimum inhibitory concentration (MIC), a clinical metric used to determine susceptibility of a pathogen to a given antibiotic compound (Figure 1a)<sup>16</sup>. Our protocol involves daily exposures of an antibiotic at a dose corresponding to its reported peak serum concentration in human patients, with durations optimized to achieve approximately 99.9% initial killing of the sensitive

parent bacteria (Figure 1b). In contrast, conventional laboratory evolution protocols start at sub-MIC concentrations to keep cultures viable and gradually increase the antibiotic dose as resistance evolves often with large dilution steps. While these protocols effectively select for resistance and have provided valuable insights, they do not realistically reflect targeted strong selection under clinically relevant antibiotic regimens<sup>7,17,18</sup>. Here, the doses we used were 8.1 µg/ml of levofloxacin, 69 µg/ml of amikacin, and 129 µg/ml of cefepime<sup>19-21</sup>. These doses are much higher than the MIC values of the parent strain (Levofloxacin: ~0.11 µg/ml; Amikacin: ~47.08 µg/ml; Cefepime: ~0.18 µg/ml, Figure 2b-d, Supplemental Figure 1b). Throughout the evolution experiments, we sampled the populations daily to quantify survival by counting colony forming units (CFUs) before and after antibiotic exposure. Antibiotics were removed by washing, and the surviving bacterial populations were transferred to antibiotic-free growth media (LB: Lysogeny Broth) for overnight growth. The next day, a modest 10-fold dilution and outgrowth primed the population for the next antibiotic exposure to avoid significant population bottlenecks and loss of diversity which are common in many evolution experiments<sup>22,23</sup> (Figure 1c). This protocol was repeated over several weeks until bacterial populations largely survived (>30 percent) their daily antibiotic exposure as measured by percent survival calculated from CFU counts before and after treatment.

The initial killing was strong for each antibiotic. Average survival on Day 1 to levofloxacin, amikacin, and cefepime was  $0.029 \pm 0.02\%$ ,  $0.058 \pm 0.11\%$ ,  $0.527 \pm 0.49\%$ , respectively ( $n = 10$ ; Figure 1d-f). As the daily selection cycles continued, levofloxacin and amikacin treatments produced survival trajectories that rapidly increased with a sigmoidal shape toward robust average survivals of  $97.2 \pm 51.8\%$  and  $163.7 \pm 116.9\%$  after 16 and 14 treatment days, respectively (Figure 1d-e). Cefepime treatment ultimately led to a treatment failure equivalent. Unlike survival trajectories for populations evolved under the selection of levofloxacin or amikacin where the trajectories had sigmoidal shapes, those observed in cefepime treatment gradually increased toward a muted survival with a mean survival of  $33.8 \pm 25.1\%$  despite 20 treatment days (Figure 1f). There was also more daily variation in survival among the individual trajectories relative to what was observed in levofloxacin and amikacin evolution experiments.

### **Evolution under selection with either levofloxacin or amikacin generates resistance with distinct cross-resistance and collateral sensitivity profiles.**

We assessed if increased bacterial survival was linked to known antibiotic resistance mechanisms. We generated dose response curves for each culture of evolved and parent cohorts in all three antibiotics to quantify cross resistance or collateral sensitivity (Figure 2a). Both MIC and inhibitory concentrations that reduced bacterial growth by half ( $IC_{50}$ ) were determined (Supplemental Figure 1, Methods). While MIC is a standard readout in clinical settings, the  $IC_{50}$  calculations are generally more robust to subtle variations in susceptibility because of better sampling at higher and lower concentrations<sup>24</sup>. At baseline, the unevolved parent strain (MG) had an average  $IC_{50}$  of  $3.07 \pm 0.77$  µg/ml in amikacin,  $0.037 \pm 0.009$  µg/ml in levofloxacin, and  $0.039 \pm 0.006$  µg/ml in cefepime (Figure 2b-d).

Evolution under the selection of amikacin ( $MG^{AMI}$ ) resulted in highly significant resistance toward amikacin with the average  $IC_{50}$  increasing ~12.7-fold to  $38.86 \pm 16.04$  µg/ml ( $p = 7.8 \times 10^{-5}$ , student's t-test) (Figure 2b). Modest but statistically significant collateral sensitivities (reductions in  $IC_{50}$ ) were observed toward levofloxacin ( $IC_{50}$ :  $0.028 \pm 0.005$  µg/ml,  $p = 0.012$ ) (Figure 2c) and cefepime ( $IC_{50}$ :  $0.031 \pm 0.007$  µg/ml,  $p = 0.037$ ) (Figure 2d).

Evolution under the selection of levofloxacin ( $MG^{LEV}$ ) resulted in highly significant resistance toward levofloxacin with the average  $IC_{50}$  increasing ~37.5-fold to  $1.37 \pm 0.53$  µg/ml ( $p = 2.4 \times 10^{-5}$ , student's t-test) (Figure 2c). No change in amikacin resistance was observed ( $IC_{50}$ :  $3.17 \pm 1.25$  µg/ml,  $p = 0.829$ ) in populations evolved under levofloxacin selection (Figure 2b). However, mild cross resistance to cefepime was observed with an average  $IC_{50}$  of  $0.082 \pm 0.024$  µg/ml ( $p = 7.0 \times 10^{-4}$ ) (Figure 2d).

## Evolution under the selection of cefepime promotes tolerance and persistence, revealing distinct survival phenotypes.

To our surprise, cultures evolved under cefepime selection ( $\text{MG}^{\text{CEF}}$ ) failed to produce robust resistance to cefepime. The  $\text{IC}_{50}$  of cefepime rose only modestly (<2-fold) to  $0.067 \pm 0.029 \mu\text{g/ml}$  ( $p = 0.014$ ) (Figure 2d). Additionally, no significant changes in cross resistance were observed toward amikacin ( $\text{IC}_{50}$ :  $3.39 \pm 0.89 \mu\text{g/ml}$ ,  $p = 0.288$ ) (Figure 2b) or levofloxacin ( $\text{IC}_{50}$ :  $0.043 \pm 0.016 \mu\text{g/ml}$ ,  $p = 0.324$ ) (Figure 2c).

In the absence of cefepime resistance, we asked whether bacterial survival in the presence of an extremely high cefepime concentration (>700 times higher than MIC) was instead due to a noncanonical survival mechanism such as antibiotic tolerance or persistence. In antibiotic tolerance (Supplementary Figure 2), the entire bacterial population survives longer under antibiotic exposure due to a slower killing rate, despite having the same MIC as antibiotic-sensitive bacteria<sup>25</sup>. Persistence, on the other hand, arises from the presence of a subpopulation of bacteria (approximately 0.1–1%) that survives antibiotic exposure by dying at a slower rate, leading to a biphasic killing curve (Supplementary Figure 2). Unlike tolerance and resistance, which affect the entire population, persistence is often considered to be associated with transient, non-heritable transcriptional shifts rather than permanent genetic changes, although mutations associated with persistence phenotypes have been reported<sup>25–28</sup>. Both tolerance and persistence are clinical concerns because standard antibiotic susceptibility tests cannot distinguish them from antibiotic-sensitive bacteria, as their MIC values are typically similar. Meanwhile, their slower killing rates pose significant challenges for effective treatment.

Minimum duration for killing (MDK) measurements were previously proposed to identify and quantitatively differentiate these phenotypes (Supplementary Figure 2)<sup>25</sup>. To perform these measurements, cultures undergoing a continuous high-dose antibiotic treatment are periodically sampled for survival (measured by CFU counts) to determine the surviving fraction relative to the untreated cultures. Over 7 hours, we monitored the killing effects experienced by the parent strain (MG) and cefepime evolved ( $\text{MG}^{\text{CEF}}$ ) cultures (Figure 2e). A strong killing effect in MG cultures was observed at 1 hour and 2 hours with surviving fractions of  $10^{-4}$  and  $10^{-6}$ , respectively (Figure 2e, black line). Killing seemingly slowed toward the end due to limits of our detection method but continued through 7 hours. Three  $\text{MG}^{\text{CEF}}$  cultures (numbers 1, 3, and 9) exhibited a biphasic shift in the killing effect at 1 hour in response to the treatment indicative of a persistence phenotype (Figure 2e, pink lines). A cohort of five  $\text{MG}^{\text{CEF}}$  cultures (numbers 2, 4–6, 10) exhibited a characteristically tolerant phenotype (Figure 2e, teal lines) with a steady and slow killing effect. Among the tolerant cultures, the killing rate varied slightly and may reflect unique means of producing the phenotype with distinct genetic changes. Two  $\text{MG}^{\text{CEF}}$  cultures (numbers 7 and 8) have a biphasic switch at the 1-hour time point indicative of persistence, but the survivor fraction was much larger than the previously described persistent cohort. With one hour survivor fractions of  $\sim 10^{-2}$ , these cultures appear to have a larger persistent subpopulation or an intermediate phenotype with characteristics of both persistence and tolerance (Figure 2e, maroon lines).

Questions emerged regarding these unexpected survival phenotypes. First, we wanted to assess the evolution of this phenotype relative to bona fide resistance typically observed in laboratory evolution experiments. To evolve cefepime resistant *E. coli* populations ( $\text{MG}^{\text{CEF,R}}$ ), we used a conventional laboratory evolution protocol and evolved six replicate isogenic cultures of MG under the selection of cefepime. We grew the cultures in a dilution series of cefepime concentrations, and each day, for 15 days, we propagated the cultures surviving in the highest concentrations allowing growth into increasingly higher concentrations of antibiotic. On the first day the average maximum allowable concentration for growth was  $0.5 \mu\text{g/ml}$  of cefepime. On day 15, the average maximum allowable concentration had risen to  $25.6 \mu\text{g/ml}$  of cefepime (Supplemental Figure 3a). This resulted in significant resistance to cefepime with the average  $\text{IC}_{50}$  rising ~227-fold to  $8.85 \pm 8.37 \mu\text{g/ml}$  ( $p = 0.027$ ) with the variance dominated by one outlier (Supplemental Figure 3d). There was also cross resistance to levofloxacin ( $\text{IC}_{50}$ :  $0.146 \pm 0.061 \mu\text{g/ml}$ ,  $p = 0.001$ ) (Supplemental Figure 3c), but limited effects on amikacin susceptibility ( $\text{IC}_{50}$ :  $5.95 \pm 3.46 \mu\text{g/ml}$ ,  $p = 0.057$ ) (Supplemental Figure 3b).

We also tested whether this protocol-related effect could be generalized beyond our laboratory strain and if the outcomes could be considered clinically relevant. Previously in our lab, a clinical, non-pathogenic *E. coli* isolate (PEc) was genetically barcoded (PbEc, abbreviated here as Pb) and used to evaluate the evolution of resistance and persistence to cefepime in mice<sup>5</sup>. In that study, *in vitro* evolution assays using the conventional protocol were also conducted and produced bona fide cefepime resistance (Pb<sup>CEF-R</sup>). We evolved six cultures of Pb under the selection of cefepime using our present protocol for 15 days (Pb<sup>CEF</sup>). Like its MG<sup>CEF</sup> counterpart, we found that the survival trajectory of Pb<sup>CEF</sup> was gradual toward muted survival (Supplemental Fig 4a), and there was no increase in cefepime resistance. Cefepime IC<sub>50</sub> actually decreased slightly from  $0.045 \pm 0.011 \mu\text{g/ml}$  at baseline (Pb) to  $0.036 \pm 0.008 \mu\text{g/ml}$  in Pb<sup>CEF</sup> ( $p=0.043$ ) whereas Pb<sup>CEF-R</sup> had an IC<sub>50</sub> of  $0.82 \mu\text{g/ml}$  (Supplemental Fig 4d). No changes were observed in IC<sub>50</sub> of amikacin or levofloxacin (Supplemental Figure 4b-c). Instead, MDK assays revealed distinct tolerant and persistent cohorts among evolved populations (Pb<sup>CEF</sup>, Supplemental Fig 4e).

### Amikacin resistance is associated with *fusA* and *trkH* mutations.

We employed population whole genome sequencing (Methods) of bulk cultures, both evolved and parent, to identify mutations and their frequencies within and among the replicate evolved populations.

All ten amikacin evolved (MG<sup>AMI</sup>) cultures shared a single high frequency mutation of *fusA*, a gene which encodes ribosomal elongation factor G that processes the translocation of the ribosome during translation and has been associated with aminoglycoside resistance<sup>7,9</sup>. The single mutation observed led to an amino acid substitution of FusA P610L. Additionally, *trkH*, a gene encoding a potassium ion transporter, was a common mutational target. Eight of ten cultures had at least one of eight unique TrkH mutations: L80Q, T20P, G156C, V155E, S105Y, Q159H, L185Q, or a 9-nucleotide deletion causing a frameshift after codon 385. TrkH L80Q was the most common and present in five of ten cultures (Figure 2f). TrkH mutations in aminoglycoside resistant bacteria and their association with collateral sensitivity were previously reported by several groups including ours<sup>9,29</sup>. Additional disparate mutations were observed among the replicate cultures (Supplemental Figure 5a). Of note, the few mutations that arose in bacterial cultures propagated without antibiotics were excluded from these analyses as they are most likely associated with adaptation to our growth conditions (Supplemental Figure 6b).

### Levofloxacin resistance is associated with *gyrA* mutations and diverse secondary mutations.

All levofloxacin evolved (MG<sup>LEV</sup>) cultures had a mutation of *gyrA* which encodes for the DNA gyrase enzyme, a target of levofloxacin. This was an expected result consistent with previous reports<sup>30</sup>. Five unique mutations were observed: GyrA G81D, GyrA S83L, GyrA S83W, GyrA A119E, and GyrA D87Y, ordered by highest occurrence (Figure 2g). In addition to GyrA mutations, six MG<sup>LEV</sup> cultures had a synonymous mutation of isocitrate dehydrogenase<sup>31-33</sup> (*icd*: Icd H366H, cac → cat), and nine cultures had a mutation of RNA polymerase beta subunit<sup>34</sup> (*rpoB*: RpoB H1237L, indel, D1064N, D1064G, E562D, and M129R). Culture 2 had both RpoB D1064N and the *rpoB* indel (Figure 2g). Many other mutations color the mutational landscape of MG<sup>LEV</sup> cultures with no distinct pattern. (Supplemental Figure 5b). Interestingly, we have not observed efflux related mutations in levofloxacin resistant cultures even though such mutations are common in cultured evolved in the presence of gradually increased levofloxacin or ciprofloxacin concentrations<sup>7</sup>.

### Evolution under Cefepime selection reveals divergent genetic changes.

Genetic trajectories in cefepime evolved (MG<sup>CEF</sup>) cultures were highly divergent, resulting in numerous unique mutations and idiosyncratic genetic changes (Figure 2h). Mutations in MG<sup>CEF</sup> cultures were predominantly found at low frequencies (~10-25%, Supplemental Figure 5c) and only few mutations were

present in multiple cultures. Two genes, *prs* and *phoQ*, were common mutational targets among subsets of MG<sup>CEF</sup> cultures. Unlike the complete penetrance of *gyrA*, *fusA* and *trkH* mutations in their respective MG<sup>LEV</sup> and MG<sup>AMI</sup> cultures, *prs*, encoding PRPP synthase (ribose-phosphate pyrophosphokinase), had five unique mutations (A114V, R79C, A76V, A11S, and I151T) present in five of the ten MG<sup>CEF</sup> cultures, with no single mutation occurring in more than two cultures (Figure 2h). Likewise, *phoQ*, encoding a transmembrane histidine kinase, had four unique mutations (G39C, an indel, and two different mobile insertion elements) each present in only one MG<sup>CEF</sup> culture (Figure 2h). Mutations of *prs* correspond to MG<sup>CEF</sup> cultures observed as having a tolerant phenotype in the MDK assay (Figure 2e), consistent with previous reports<sup>35</sup>. No pattern between mutations of *phoQ* and a survival phenotype was apparent. Many additional disparate mutations were present in MG<sup>CEF</sup> cultures (Supplemental Figure 5c).

MG<sup>CEF-R</sup> populations, in contrast, evolved using the conventional resistance evolution protocol, had convergent evolution toward mutations in genes associated with beta lactam resistance including peptidoglycan transpeptidase<sup>36</sup> (*ftsI*) and with multidrug resistance including outer membrane porin C<sup>37</sup> (*ompC*), an *ompC* repressor, *envZ*<sup>36,38</sup>, efflux pump gene *acrB* of the *acrAB* operon, its repressor *acrR*<sup>36,39</sup>, and the *marR* repressor of the multiple antibiotic resistance operon(*marRAB*)<sup>40,41</sup> (Supplemental Figure 3e). These differences in mutational outcomes relative to evolution protocol were also observed in Pb<sup>CEF</sup> and Pb<sup>CEF-R</sup> (Supplemental 4f).

### **Sequential treatments with all three antibiotics ultimately result in treatment failure despite initial susceptibility and collateral sensitivity.**

We analyzed the outcomes of single-antibiotic treatments to design a rational sequence for multiple-antibiotic therapy. MG<sup>LEV</sup> cultures remained sensitive to amikacin but had elevated resistance to cefepime, leaving only amikacin as a viable continuation for this cohort (Figure 2b, d). Meanwhile, MG<sup>AMI</sup> cultures had small but statistically significant collateral effects on sensitivity to levofloxacin and cefepime, leaving both antibiotics as viable options (Figure 2c-d). Previous studies have reported on the collateral effects of aminoglycoside toward beta lactams<sup>9,19</sup>, so we hypothesized that using amikacin to treat MG<sup>LEV</sup> cultures would resensitize them to cefepime as we observed in MG<sup>AMI</sup> cultures.

Based on this rationale, we evolved the terminal MG<sup>LEV</sup> cultures under the selection of amikacin (MG<sup>LEV,AMI</sup>) daily until there was sustained survival, and then we evolved those cultures under the selection of cefepime (MG<sup>LEV,AMI,CEF</sup>) toward the same endpoint. The evolution protocol, dosing, and durations were the same as their single antibiotic treatment counterparts.

The initial killing by amikacin was strong as we anticipated. The average survival on Day 1 (17th cumulative treatment day) was  $0.356 \pm 0.858\%$  (Figure 3a). However, we observed an increase in the phenotypic diversity of response relative to day one of the prior levofloxacin treatment. This was justified as the terminal MG<sup>LEV</sup> cultures entered the new treatment with greater genetic diversity than the isogenic parent strain (MG) in our initial experiments. The survival trajectories increased rapidly in a sigmoidal pattern, leading to robust survival. After 15 days of amikacin evolution (31 days in total), the cultures had an average survival of  $102.25 \pm 56.44\%$ , so we initiated the cefepime treatment. The strong killing effect was restored by cefepime on day 1 (32<sup>nd</sup> cumulative treatment day) with an average survival of  $0.271 \pm 0.292\%$ , and the diversity of responses again grew. Like its single antibiotic treatment counterpart (Figure 1f), the survival trajectories through cefepime were gradual and toward an average modest survival of  $39.77 \pm 34.73\%$  even after 50 cefepime treatment days (81 days in total) (Figure 3a).

### **Sequential evolution induces amikacin resistance, maintains cefepime sensitivity, and resensitizes to bacteria to preceding antibiotics.**

Evolved bacterial cultures from the final days of each segment of the sequential antibiotic evolution were evaluated for resistance across all three antibiotics (Figure 3b-d, Supplemental Figure 7). Following the amikacin segment of the sequential evolution, MG<sup>LEV,AMI</sup> cultures were significantly more resistant to amikacin with an average IC<sub>50</sub> of  $26.228 \pm 7.864 \mu\text{g/ml}$  of amikacin, an ~8-fold change ( $p = 4 \times 10^{-6}$ ) relative to MG<sup>LEV</sup> cultures (Figure 3c). MG<sup>LEV,AMI</sup> cultures were also moderately resensitized to levofloxacin relative to MG<sup>LEV</sup> cultures (~2-fold) with an average IC<sub>50</sub> of  $0.615 \pm 0.426 \mu\text{g/ml}$  of levofloxacin ( $p = 5 \times 10^{-3}$ ), but MG<sup>LEV,AMI</sup> cultures remained significantly more levofloxacin resistant than parent MG cultures ( $p = 2 \times 10^{-3}$ ) (Figure 3b). As we hypothesized, evolution under the selection of amikacin significantly reversed the cross resistance to cefepime observed in MG<sup>LEV</sup>, resulting in a reduction in the average IC<sub>50</sub> from  $0.082 \pm 0.024 \mu\text{g/mL}$  in MG<sup>LEV</sup> to  $0.052 \pm 0.026 \mu\text{g/ml}$  in MG<sup>LEV,AMI</sup> ( $p=8\times10^{-3}$ ). This IC<sub>50</sub> value was also not significantly higher than the cefepime IC<sub>50</sub> in the parent MG cultures ( $0.039 \pm 0.006 \mu\text{g/ml}$  cefepime,  $p = 0.158$ ) (Figure 3d).

After evolution under the selection of cefepime (MG<sup>LEV,AMI,CEF</sup>), levofloxacin resistance rose slightly but not significantly relative to MG<sup>LEV,AMI</sup> to an average IC<sub>50</sub> of  $0.754 \pm 0.559 \mu\text{g/ml}$  of levofloxacin ( $p = 0.3$ ) (Figure 3b). MG<sup>LEV,AMI,CEF</sup> was significantly resensitized to amikacin relative to MG<sup>LEV,AMI</sup> where the average amikacin IC<sub>50</sub> dropped to  $9.420 \pm 6.152 \mu\text{g/ml}$  from  $26.228 \pm 7.864 \mu\text{g/ml}$  ( $p = 1 \times 10^{-4}$ ) (Figure 3c). This interaction was not observed in the single antibiotic treatment counterpart (MG<sup>CEF</sup>). Ultimately, MG<sup>LEV,AMI,CEF</sup> had no change in cefepime resistance relative to MG<sup>LEV,AMI</sup> with an average IC<sub>50</sub> of  $0.571 \pm 0.024 \mu\text{g/ml}$  ( $p = 0.395$ ) (Figure 3d). Rather, MDK assays with MG<sup>LEV,AMI,CEF</sup> cultures revealed that the increased survival was associated with persistence and tolerance phenotypes (Figure 3e). Two MG<sup>LEV,AMI,CEF</sup> cultures (numbers 2 and 5) were characteristically tolerant (Figure 3e, teal lines). Two cultures (numbers 3 and 8) had an intermediate phenotype (Figure 3e, maroon lines). The remaining six cultures (numbers 1, 4, 6, 7, 9, and 10) were characteristically persistent (Figure 3e, pink lines) with a biphasic killing curve. The shift occurred at survivor fractions between  $10^{-2}$  and  $10^{-3}$  indicating relatively large persistent subpopulations (Figure 3e). The mix of alternative survival strategies was similar to what was observed in MG<sup>CEF</sup> cultures (Figure 2e) and Pb<sup>CEF</sup> cultures (Supplemental 4e).

### **Evolution under the sequential use of antibiotics, as treatments fail, favors GyrA S83L over other GyrA mutations through adaptive selection in diverse populations.**

Next, we asked how the evolutionary context and history impacted mutational routes toward survival by Illumina whole sequencing of frozen samples isolated from evolved cultured at different time points. When we tracked the five GyrA mutations of MG<sup>LEV</sup> through the subsequent evolutions under the selection of amikacin and cefepime, we observed that GyrA S83L had an advantage in the amikacin treatment regime where it was either fixed or it replaced the previously dominant GyrA mutations (Figure 4a, Supplemental Figure 8a). Notably, because we maintain population diversity, mutations with initially undetectable frequencies in our sequencing-based assay can emerge by replacing other mutations. Strikingly, by day 34, S83L was the dominant GyrA mutation across all cultures. Mutations of RpoB on the other hand were selected against during amikacin treatment (Supplemental 8b). In all but culture number 2, RpoB mutations became nearly undetectable by the conclusion of amikacin treatment (day 31). In culture 2, the *rpoB* indel survived amikacin treatment, but subsequently was selected against through cefepime treatment. The synonymous Icd H366H mutation, present in only six MG<sup>LEV</sup> cultures, emerged in all cultures throughout the full sequential treatment regime with momentary losses of its detection at various time points in eight cultures (Supplemental 8b).

### **Sequential evolution drives distinct *fusA* diversity followed by extinction, and TrkH L185Q fixation under amikacin and cefepime treatments.**

Like MG<sup>AMI</sup>, MG<sup>LEV,AMI</sup> cultures acquired mutations in *fusA* and *trkH* genes, yet the number and type of mutations differed. Where MG<sup>AMI</sup> cultures had only the FusA P610L mutation, MG<sup>LEV,AMI</sup> cultures had 11 unique FusA mutations. This difference was most likely due to greater initial population diversity of

MG<sup>LEV</sup> cultures before amikacin selection started. The 11 mutations included the P610L mutation, although here P610L was observed in only two cultures. Interestingly, P610L and the other 10 FusA mutations (G46C, R59H, I61M, V116F, G117C, F593L, F605L, A608V, P610T, and A678V) failed to maintain high frequencies and were subsequently driven to extinction by the final cefepime treatment day (Figure 4a, Supplemental Figure 8c), indicating a potential fitness cost under cefepime treatment.

Alternatively, where MG<sup>AMI</sup> cultures had eight different TrkH mutations, MG<sup>LEV,AMI</sup> cultures had only three: T20I, L80Q, and L185Q. In striking contrast, L185Q was the dominant TrkH mutation in MG<sup>LEV,AMI</sup> cultures. Previously, only one MG<sup>AMI</sup> culture had the L185Q mutation, and it was at a low frequency (0.11). All ten MG<sup>LEV,AMI</sup> cultures had the L185Q mutation, and it was quickly fixed throughout amikacin treatment and maintained in the subsequent cefepime treatment (Figure 4a, Supplemental Figure 8d). Only culture number 2 diverged from this pattern where L185Q did not emerge until after the switch to cefepime and failed to fix. Survival of this culture through amikacin selection may have instead been supported by the FusA F593L mutation. FusA F593L was present in three cultures, making it the most common among the 11 FusA mutations and it occurred at high frequencies (0.5) relative to the other FusA mutations in MG<sup>LEV,AMI</sup> cultures, indicative of a higher relative fitness.

Culture number 9 had the only TrkH L80Q mutation in MG<sup>LEV,AMI</sup> cultures, and it was fixed by the final amikacin treatment day (Day 31). When the treatment was switched to cefepime, L80Q was quickly replaced by L185Q, which was likely present at a frequency below the limit of detection. Following three days of cefepime (Day 34), frequency of L80Q dropped to 0.08, and the frequency of L185Q was 0.884. By day 47, L80Q was undetectable and L185Q was fixed (Supplemental Figure 8d).

### Cefepime-induced selection following sequential treatments with levofloxacin and amikacin drives convergent evolutionary trajectories.

The evolution of survival under the selection of cefepime in MG<sup>LEV,AMI,CEF</sup> cultures was markedly convergent. In contrast to the divergent evolution observed in MG<sup>CEF</sup>, each of the ten MG<sup>LEV,AMI,CEF</sup> cultures acquired nearly identical mutations among a set of nine genes at various times (Figure 4, Supplemental Figure 8e). Among the nine mutations were GyrA S83L and TrkH L185Q, which were inherited from previous selection regimens under levofloxacin and amikacin. The additional mutations emerged with a variable cadence across individual cultures (Figure 4b). Concurrent to TrkH L185Q, a single nucleotide deletion in *glvC*, a poorly characterized putative phosphoenolpyruvate (PEP)-dependent carbohydrate transport system (PTS) component<sup>42,43</sup>, evolved with nearly identical frequencies indicating a common clade and positive selection for the mutated *glvC*. The deletion occurred at nucleotide 1042 of 1072 generating a downstream stop codon that likely truncates the protein by 17 amino acids.

Next, emerged two other concurrent mutations in *selB* and intergenically between *fimB* and *fimE* (*fimB/E*). *selB*, encoding a translation factor involved in incorporation of selenocysteine into proteins<sup>44</sup>, had a 2-nucleotide insertion that created a frame shift at amino acid 494 and an early stop codon at 526, possibly truncating what is typically a 614 amino acid protein. *fimE*, a regulatory gene that, with *fimB*, controls the production of type 1 fimbriae<sup>45</sup>, was likely lost following an IS5 mobile insertion element inserting between the *fimE* promoter and its transcription start site<sup>46</sup>. This mutation pair was observed in all cultures beside number 2, and either emerged with TrkH L185Q and the mutated *glvC* or after.

All MG<sup>LEV,AMI,CEF</sup> cultures subsequently had a 7-nucleotide long deletion in *rpoZ*, which encodes the omega subunit of RNA polymerase. The deletion occurs relatively early in the gene (68-74 of 276 nucleotides) and introduces an early stop codon after just 29 amino acids, a severe truncation of what is typically a 91 amino acid protein. A mutation of *hipA* (HipA P86L), a gene named for its association with a highly persistent phenotype, was observed in all but culture 2<sup>26</sup>. Additionally, mutations of *ftsH*, a gene encoding a membrane-bound protease involved in stress response<sup>47,48</sup>, and of *gatA*, a known galactitol-specific component of the PTS system<sup>49,50</sup> were observed in all cultures besides numbers 2, 9, and 10. The *ftsH* gene incurs an in-phase deletion of 12 nucleotides removing codons 261-264 of 644 within its AAA+

domain. *gatA*, meanwhile is disrupted by the mobile insertion element IS5 following its 69<sup>th</sup> amino acid (Figure 4b).

By the final day many of the discussed mutations were present at high frequencies and those below total fixation shared the frequency of others indicating their concurrence within a common clade (Figure 4c).

The shift from divergent evolution under the selection cefepime as a single treatment in MG<sup>CEF</sup> toward convergent evolution when cefepime was used a sequential treatment in MG<sup>LEV,AMI,CEF</sup> was striking and not previously reported to best of our knowledge. The result echoes the observation in the number of FusA and TrkH mutations afforded to MG<sup>AMI</sup> (FusA: 1; TrkH: 8) and MG<sup>LEV,AMI</sup> (FusA: 11,TrkH: 3) cultures. These shifts are illustrated in Figure 4d where bacterial populations evolve under the selection of an antibiotic (color) through various mutational options (arrows) given the single vs sequential context of the evolution. Many mutations within evolved populations are driven to extinction within subsequent antibiotic exposures. The full breadth of mutations within the cohorts of evolved cultures following single and sequential evolutions are shown in Supplemental Figure 8. The choice was made to exclude MG<sup>LEV,AMI,CEF</sup> cultures 2, 3, and 8 from this figure as each had exceedingly numerous mutations associated with a mutation of *mutL*. Further, the *mutL* mutation was first identified in culture number 2 during the amikacin regime. Later, on day 81, *mutL* was observed in cultures 3 and 8 along with other mutations present in culture 2, making it difficult to rule out a possible contamination of those cultures sometime between days 63 and 81.

### **Individual convergent mutations are insufficient alone to produce persistence suggesting a supporting role in HipA led phenotype.**

The convergent clade mutations, whether considered together or individually, may confer pleiotropic fitness effects, particularly those involving insertions and deletions, which are likely to significantly impact molecular interactions or gene regulation. While each mutation requires systematic functional studies, the large number of identified mutations and the vast combinatorial space of their potential interactions make genetic confirmation of all 9 mutation combinations impractical at present. Therefore, we evaluated the mutations individually for their effects on survival.

We genetically introduced the mutations to the wild-type, parental MG1655 (MG) using oligo recombineering and oligo-recombineering-followed-by-Bxb-1-Integrase-Targeting (ORBIT)<sup>51</sup>. Oligonucleotides were designed for each mutation to reproduce what was observed in the evolved populations (Supplementary Table 1). The single nucleotide substitution in *hipA*, the single nucleotide deletion in *glvC*, the two-nucleotide insertion in *selB*, and the 7- and 12-nucleotide deletions of *rpoZ* and *ftsH* were encoded at the center of their respective oligonucleotides with flanking regions of perfect homology to the reference genome. Mutations of *gatA* and *fimE* were the result of transposon insertions and required a different approach in the oligonucleotide design. The transposon insertion in *gatA* bisected the gene following the 69<sup>th</sup> amino acid with an unknown effect on the final protein product. To make this mutation, the oligonucleotide was designed to introduce a stop codon following the 69<sup>th</sup> amino acid, truncating the protein. The transposon insertion of *fimE* occurs between its promoter and transcription start site, and this precise mutation event has been shown to knockout its expression<sup>46</sup>. In this case, ORBIT was used to fully delete the *fimE* gene. Mutants were screened using mutant-specific PCR primers (Supplementary Table 2) and confirmed by Sanger sequencing. The strains produced from this mutagenesis are referred to going forward as their parent strain background (MG) with the mutated gene in superscript (e.g., MG<sup>gatA</sup>, MG<sup>glvC</sup>).

Next, the mutants were phenotypically evaluated for changes in their growth, susceptibility to antibiotics (MIC), and survival by persistence or tolerance in the presence of cefepime (MDK assay, Supplementary Figure 2). Contributions to survival from slower growth was evaluated as it might lend to tolerance<sup>52</sup>. The parent strain (MG) had a mean doubling time of  $20.07 \pm 0.80$  minutes (Figure 5a). The mutations had limited effects on growth. The doubling times were  $21.17 \pm 0.92$  minutes for MG<sup>gatA</sup> ( $p = 0.0501$ ), 20.83

$\pm 0.51$  minutes for MG<sup>glvC</sup> ( $p = 0.0782$ ),  $20.31 \pm 1.29$  minutes for MG<sup>hipA</sup> ( $p = 0.7080$ ),  $21.62 \pm 0.41$  minutes for MG<sup>selB</sup> ( $p = 0.0017$ ),  $21.91 \pm 0.88$  minutes for MG<sup>rpoZ</sup> ( $p = 0.0036$ ),  $20.18 \pm 1.07$  minutes for MG<sup>ftsH</sup> ( $p = 0.8362$ ), and  $21.66 \pm 0.57$  for MG<sup>fimE</sup> ( $p = 0.0026$ ).

In the absence of major growth defects, we tested resistance of the individual mutant strains to levofloxacin, amikacin, and cefepime to see if they contribute to the phenotypes observed in the diverse mutational backgrounds. As before, IC<sub>50</sub> and MIC were estimated from growth data following overnight growth at 37°C in a range of antibiotic concentrations. The values estimated for the parent strain in this iteration of the assay were comparable to earlier experiments with IC<sub>50</sub> values of  $0.037 \pm 0.001$  µg/mL levofloxacin,  $3.632 \pm 0.853$  µg/mL amikacin, and  $0.035 \pm 0.010$  µg/mL cefepime (Figure 5b-d). MIC for the parent strain was estimated to be  $0.077 \pm 0.009$  µg/mL levofloxacin,  $58.102 \pm 17.998$  µg/mL amikacin, and  $0.152 \pm 0.136$  µg/mL cefepime (Supplementary Figure 10a-c). Most of the individual mutations (MG<sup>gatA</sup>, MG<sup>glvC</sup>, MG<sup>rpoZ</sup>, and MG<sup>fimE</sup>) did not affect resistance to any of the three antibiotics (Figure 5b-d). Rather, both MG<sup>hipA</sup> and MG<sup>selB</sup> had a slightly higher IC<sub>50</sub> in levofloxacin with values of  $0.055 \pm 0.004$  µg/mL ( $p=0.014$ ) and  $0.089 \pm 0.020$  µg/mL ( $p=0.046$ ), respectively (Figure 5c). The MIC change of MG<sup>hipA</sup> in levofloxacin was also significant at  $0.171 \pm 0.008$  µg/mL ( $p=0.0002$ ) (Supplemental Figure 10b). The MIC of MG<sup>selB</sup> was elevated as well to  $0.347 \pm 0.214$  µg/mL ( $p=0.159$ ), but it was not significant due to more variation among the replicates, and MG<sup>ftsH</sup> was significantly but modestly elevated to  $0.100 \pm 0.005$  µg/mL levofloxacin ( $p=0.028$ ) (Supplementary Figure 10b). MG<sup>selB</sup> was significantly resistant to amikacin indicated by elevated IC<sub>50</sub> to  $12.29 \pm 1.42$  µg/mL ( $p=0.002$ ), while MG<sup>ftsH</sup> was mildly sensitized to amikacin with an IC<sub>50</sub> of  $1.722 \pm 0.431$  µg/mL ( $p=0.04$ ) (Figure 5b).

The result indicating that none of the individual mutations had effects on cefepime resistance is consistent with absence of an effect on cefepime resistance within the diverse, evolved MG<sup>LEV,AMI,CEF</sup> populations, where the cultures survived by persistence and tolerance. The effects of MG<sup>hipA</sup> and MG<sup>selB</sup> on levofloxacin resistance reflect the mildly, non-significant cross-resistance to levofloxacin following the terminal cefepime treatment in the sequential antibiotic evolution (MG<sup>LEV,AMI,CEF</sup>). The terminal cefepime treatment had a collateral sensitivity effect on amikacin, but here the result is mixed. MG<sup>selB</sup> was resistant to amikacin by 3.38-fold relative to MG.

Next, we used the MDK assay to identify the impact of the mutations on survival by tolerance and persistence. The parent strain (MG) is quickly killed by the effects of cefepime in the first hour with a surviving fraction just above  $10^{-4}$  (Figure 5e). Many of the mutant strains were killed at the same rate as parent MG through each timepoint. Only MG<sup>hipA</sup> was less susceptible through 1 hour with a surviving fraction of  $10^{-3}$ . MG<sup>fimE</sup> was also slightly elevated, perhaps an effect of its longer doubling time, but it was an effect that did not persist throughout the remainder of the MDK assay. The rate of killing slowed considerably for MG<sup>hipA</sup> relative to MG and the other mutants and continued to have roughly 10-fold greater survival at every time point. Ultimately after 7 hours, MG<sup>hipA</sup> had a surviving fraction above  $10^{-5}$ , while the other cultures were at or below  $10^{-6}$ . The biphasic shift in its killing is indicative of persistence, reflecting previous observations of the phenotype in *hipA* mutants.

The relatively high frequencies and penetrance of other mutations among the replicate MG<sup>LEV,AMI,CEF</sup> populations suggest a positive effect on fitness in the presence of cefepime. This observation strongly indicates that their contribution to survival and fitness is either epistatic in nature or acts in support of the HipA-led phenotype. Indeed, when the survival of MG<sup>hipA</sup> is directly compared to that of a diverse, evolved culture, MG<sup>LEV,AMI,CEF-7</sup>, the presence of additional mutations is associated with enhanced survival. A similar pattern was observed in MG<sup>prs</sup>, a strain engineered with the Prs A114V mutation, and its corresponding diverse, evolved culture, MG<sup>CEF-5</sup> (Supplemental Figure 10d).

In summary, both *hipA* and *prs* mutations display persistence and tolerance phenotypes, respectively. However, evolved cultures carrying the exact same mutations exhibit stronger persistence or tolerance

phenotypes, suggesting the presence of epistatic interactions between the mutations observed in the evolved populations. As mentioned previously, generating combinatorial libraries of these mutations is currently not feasible for us.

### Single cell RNA sequencing of evolved cultures following sequential treatment reveals

To determine how the diverse, accumulated mutations influence community composition, we used single-cell RNA sequencing (scRNASeq) to characterize changes in the gene expression landscape resulting from sequential antibiotic exposure. Samples were collected from exponentially grown cultures at the same optical density (OD=1.0) of the parent strain and two cultures that accumulated largely overlapping mutations: MG<sup>LEV,AMI,CEF</sup>-4 and MG<sup>LEV,AMI,CEF</sup>-7. Using ProBac-seq<sup>53</sup>, a probe based bacterial scRNASeq method, we analyzed a total of 48,883 single cells from duplicate samples of these three cultures (Supplementary Table 3). Using dimensionality reduction and graph-based clustering, cells were grouped into 9 unique clusters (Figure 6a). While most cell clusters included at least a few cells from each culture, there were notable instances in which specific clusters were predominantly composed of cells from distinct cultures (Figure 6b, c). Notably, the majority of cells in clusters 1 and 2 were of parental origin (>67% and >70% parent cells in each cluster, respectively). Gene-set enrichment analysis (GSEA) identifies translation-related processes and expression of ribosomal subunits as highly enriched in these clusters (Supplementary Table 3, Supplementary Figure 11) These same gene sets were enriched when comparing the wildtype to either culture without cluster-based analysis (Figure 6d, e and supplementary table 4). The signature of higher translational activity in the parent strain is consistent with the common observation that antibiotic persistence is associated with lower activity levels<sup>54</sup>.

Cells from each of the evolved cultures were commonly and significantly enriched in transcripts for the superpathway of glycolysis, pyruvate dehydrogenase, TCA, and glyoxylate bypass, with several glyoxylate shunt genes overexpressed in these cultures (shared genes in Figure 6d, e and Supplementary Table 4). Culture MG<sup>LEV,AMI,CEF</sup>-4 comprised the majority of cells in cluster 9 (>72%), which itself was enriched in this superpathway (Figure 6c, Supplementary Figure 12, Supplementary Table 4). Similarly, culture MG<sup>LEV,AMI,CEF</sup>-7 comprised over 80% of cluster 4 cells, which were enriched in this superpathway (Figure 6c, Supplementary Figure 12, Supplementary Table 4). Taken together, single cell analysis demonstrates that the evolved cultures have cells occupying distinct metabolic niches and contain fewer cells in states that are consistent with high translation activity. This pattern is in line with changes that would be expected from mutations that affect toxin-antitoxin genes including *hipA* identified here. Expression of *hipA* itself was significantly overexpressed in MG<sup>LEV,AMI,CEF</sup>-4, while in MG<sup>LEV,AMI,CEF</sup>-7 too few individual cells were profiled as having significant overexpression of *hipA*. The observation mirrors the subpopulation survival effect which is characteristic of persistence.

## **DISCUSSION**

Predicting how bacteria survive clinically relevant antibiotic treatment regimens is crucial for designing evolution-proof antibiotics and treatment strategies. Laboratory evolution experiments, whether conducted using *in vitro* or *in vivo* models, have been instrumental in advancing our understanding of antibiotic resistance evolution<sup>5,55</sup>. However, the design of these experiments can significantly influence their outcomes and may not always reflect real-world conditions<sup>56</sup>.

In this study, by mimicking the lethally high antibiotic peak doses observed in human patients, we demonstrate that treatment context, whether an antibiotic was administered as a single exposure or in sequence, had effects on shaping bacterial survival strategies at the phenotypic level. Nevertheless, we found that this treatment context drives notable differences in the mutational pathways leading to bacterial survival. We hypothesize that these differences in mutational routes could inform the development of improved clinical treatment designs.

We demonstrated that, phenotypically, use of levofloxacin and amikacin led to resistance evolution while cefepime use led to persistence and tolerance evolution, and these outcomes were independent of the single or sequential context of the treatments (Figures 2, 3). Likewise, the outcomes of persistence and tolerance were independent of the population structure (isogenic or polyclonal) and strain (MG1655 or Pb) (Figure 2, 3 and Supplemental Figure 4).

However, we observed context-specific evolution of collateral antibiotic sensitivity<sup>7-9</sup>. Amikacin as a single treatment had only minor collateral effects on sensitivity toward levofloxacin and cefepime (Figure 2c-d), but amikacin as a sequential treatment following levofloxacin substantially reversed the levofloxacin-associated cross resistance toward cefepime (Figure 3b,d). Our work builds on previous work that showed collateral sensitivities between aminoglycosides and non-aminoglycosides by demonstrating potential strategies to prime and amplify these types of interactions<sup>9,19</sup>.

Another context-specific evolutionary outcome was observed with cefepime treatment. Cefepime as a single treatment (MG<sup>CEF</sup>) had no effect on cross-resistance to amikacin (Figure 2b), but when used as a subsequent treatment following amikacin, cefepime reduced amikacin resistance of evolved populations (Figure 3c) possibly by selecting against FusA mutations (Figure 4a-ii, Supplementary Figure 8c), although this effect did not completely resensitize the populations to amikacin relative to the parent cultures. The effect of secondary antibiotics to resensitize bacteria toward a primary antibiotic has been reported<sup>57,58</sup>. We add to the line of research by tracking specific mutational routes through secondary and tertiary antibiotic treatments. With positive trends in cost and throughput of sequencing technologies, clinical decisions may be able to rely on findings of this sort in the near future<sup>59</sup>.

In this vein, we observed five well-known mutations of *gyrA* following levofloxacin treatment (Figure 2h), four of which are in the GyrA quinolone resistance-determining region (QRDR) hotspot spanning amino acids 51 and 106 where mutations affect the binding of the antibiotic to its target<sup>30,60</sup>. We then demonstrated that in sequential treatments with amikacin, across all replicate cultures, clades containing the GyrA S83L were more fit than those with the other GyrA mutations (Supplemental Figure 8a). Previously, allele-specific collateral effects of GyrA mutations were demonstrated through resistance measurements across a variety of antibiotics<sup>29</sup>. While we do not test the specific mutations for collateral effects on amikacin susceptibility, we observe the relative fitness advantage of S83L through evolution of bacteria under amikacin selection and find consistent S83L outperformance despite the abundance and diversity of additional mutations within and across replicate cultures.

Prior treatment of levofloxacin also impacted the mutational routes toward amikacin resistance. Mutations in *fusA* and *trkH* are characteristic of aminoglycoside resistance<sup>7,9</sup>. When amikacin was used as a single treatment, only one FusA mutation (P610L) emerged alongside a mix of eight TrkH mutations, dominated by L80Q (Figure 2f). When bacteria evolved first under the selection of levofloxacin, the mutational routes toward the subsequent amikacin treatment were such that eleven FusA mutations and three TrkH mutations emerged, with TrkH L185Q dominating the replicate cultures (Supplemental Figure 8c-d). As described previously, there may be allele-specific differences in collateral sensitivity networks associated with the amikacin resistance between MG<sup>AMI</sup> and MG<sup>LEV,AMI</sup>. This implicates primary antibiotic choice in dictating the range of outcomes in susceptibility to tertiary antibiotics. While no FusA mutation survived the subsequent cefepime treatment, TrkH L185Q emerged as the sole fixed TrkH mutation.

The differences in population diversity among cultures preceding the single antibiotic evolutions and within the evolved cultures through sequential antibiotic evolutions likely influence these shifts. An isogenic culture of MG, for instance, can carry throughout its evolution emerging mutations with marginal beneficial or deleterious fitness effects, but the mutations may not survive ongoing treatment due to a limited array of genetic complexity that could offer compensatory or synergistic effects. Alternatively, the diverse genetic backgrounds of evolved MG<sup>LEV</sup> and MG<sup>LEV,AMI</sup> populations as they are transitioned to amikacin and cefepime treatment, respectively, can potentiate numerous resistance-conferring and compensatory mutations.

In addition to allele-specific opportunities for antibiotic use strategies, we observed that treatment design can shift evolutionary trajectories from divergent to convergent genetic pathways. In such scenarios, evolutionary constraints such as epistasis between mutations or fitness costs of mutations in different antibiotics may trap bacteria with fewer viable mutational routes toward resistance in subsequent treatments creating an opportunity for rational treatment design. Here, when the parent MG strain evolved under cefepime selection, bacterial ( $\text{MG}^{\text{CEF}}$ ) survival was associated with numerous divergent mutational routes, each providing a unique genetic context, which clinically might complicate the subsequent treatment decisions (Figure 2h, Supplemental Figure 5c). The convergent evolution in  $\text{MG}^{\text{LEV},\text{AMI},\text{CEF}}$  of up to 9 mutations (Figure 4-iv, Supplemental Figure 8e), rather, has a relatively simpler genetic context as a population. Importantly, the prioritization of mutational landscape complexity in bacterial populations of treatment failures may not always be necessarily advantageous. At the very least, it may only be beneficial in specific antibiotic regimens. The mutations present in convergent evolution trajectories may create a treatment opportunity to leverage or may otherwise prove to be highly cross-resistant or extensively persistent and tolerant. The hypothesis that driving convergent evolution can reduce treatment failures and limit the evolution of multidrug resistance is supported by observations on the role of standing variation in adaptation to new stresses, as well as clinical findings on how strain diversity impacts resistance evolution and treatment failure<sup>61,62</sup>.

When we tested the individual convergent mutants for their contributions to survival, it was observed that only the HipA mutation was sufficient for the persistent phenotype (Figure 5e). However, the degree of survival throughout the MDK assay of  $\text{MG}^{\text{HipA}}$  was lower relative to the survival observed in MDK assays of evolved  $\text{MG}^{\text{LEV},\text{AMI},\text{CEF}}$  (Supplementary Figure 10). We hypothesize that the additional convergent mutants either contribute to survival through epistatic interactions among them. In an effort to provide support for these hypotheses, we compiled information about the mutations in these genes from the literature summarized below.

HipA is a kinase that activates persistence and the stringent response by driving the accumulation of ppGpp. The *hipA7* allele, a well characterized set of HipA mutations (G22S and D291A), exacerbates the phenotype through its preferential activity toward GltX, upstream of ppGpp accumulation. Further, HipA dimerizes and forms a complex with a HipB dimer to repress the *hipBA* operon. G22 and P86 sit at the HipA dimer interface and the respective mutations weaken the interaction, allowing greater free HipA and less transcriptional autoregulation of the operon<sup>63-67</sup>. The present mutation, HipA P86L has also been identified in laboratory and clinical isolates with similar phenotypic consequences of persistence<sup>66</sup>.

The deletion in *selB* and its likely truncation may interfere with its role in selenocysteine incorporation<sup>44</sup>. Additionally, long truncations of SelB have also been shown to regulate the translation of non-selenoproteins through a dominant negative mechanism<sup>68</sup>. While no connection between *selB* and antibiotic survival has been reported to date, it is generally accepted that inhibition of protein translation contributes to antibiotic tolerance and persistence<sup>28,54,69</sup>.

The precise disruption the *fimE* promoter by an insertion of IS5 as we observed here was reported previously and found to lock expression of type-1 fimbriae, a virulence factor, in an actively expressing state<sup>46</sup>. While no actionable fitness costs have been reported for fimbriae production, its production is energetically costly and the associated increase in adherence may limit motility<sup>70</sup>.

The role of *givC* remains unclear in the literature although it is putatively a component of PTS<sup>42</sup>. However, the full penetrance of the 1-nucleotide deletion in all 10  $\text{MG}^{\text{LEV},\text{AMI},\text{CEF}}$  cultures suggests positive selection and a role in the survival phenotype or a role in compensating fitness costs associated with its concurrent mutation, TrkH L185Q.

GatA, a verified component of PTS, along with GatB and GatC are involved in galactitol transport. The large truncation of GatA observed here may affect its interactions with GatB and the transportation and metabolism of galactitol. GatA has also been implicated in resolving acid stress whether environmental

or the outcome of carbon utilization<sup>49,50</sup>, and intracellular acidity can induce persistence and tolerance by reducing protein synthesis<sup>28</sup>.

FtsH, among its roles, degrades stress response regulators to allow bacteria to return to a prestressed state<sup>47,48</sup>, and degrades enzymes, LpxC and KdtA, involved in the early steps of LPS biosynthesis<sup>71</sup>. Interestingly, the FtsH-mediated degradation of LpxC is modulated by alarmone ppGpp<sup>72</sup>. The 4 codon deletion within the AAA+ domain may alter ATP binding or protease efficiency as a way of adapting to prolonged stress or to compensate or potentiate the HipA persistence phenotype<sup>73</sup>.

Finally, we observed a large truncation of RpoZ, the omega subunit of RNA polymerase. While the omega subunit is not essential, it interacts with the other subunits in many contexts including in the propagation of the stringent response by alarmone ppGpp contributing to a persistence phenotype<sup>74,75</sup>. The connection to HipA is further supported in the observed cadence of mutation emergence, where mutations of FtsH and RpoZ always coincide or succeed the mutation of HipA.

The results of our single cell RNA sequencing analysis reveal additional complexity within and among the evolved populations. Clustered cells with widespread expression changes of metabolic and translation programs highlight additional opportunities to characterize bacterial susceptibility following distinct treatment regimes. The analysis revealed *hipA* overexpression in a subpopulation of cells consistent with the phenotypic killing effect observed in MDK assays. As we observed allele-specific susceptibility and survival, we hypothesize that clusters of cells or expression of certain gene sets will lend to greater survival relative to whole bacterial population during antibiotic treatment. We anticipate these experiments in future studies.

Collectively and individually, these observed mutations could have profound effects on bacterial physiology and may offer new treatment strategies through the exploitation of their collateral effects. However, the clinical application of such strategies would require the emergence of these mutations in clinical settings. Until then, observations of these mutated genes generally contribute to the growing body of evidence supporting their role in antibiotic survival in cases where such associations have been reported.

This work offers an initial roadmap for identifying sequential antibiotic treatments that promote favorable mutational trajectories in the face of multiple treatment failures. Our ability to predict mutational routes toward resistance, persistence and tolerance may improve antibiotic choice based on known collateral phenotypic effects. Further, as shown here, sequential treatments can shift evolution from divergent to convergent routes where bacteria may have fewer mutational options to surviving subsequent treatments. Designing treatment paradigms to drive convergent evolution could complement designs based on collateral sensitivity by restricting the outcomes to predictable and actionable mutational routes. Additional investigations of this kind could be performed experimentally, as was done here, with more antibiotics and sequences, or rather by sequencing clinical isolates following sequential antibiotic treatment courses. Ultimately more research is required to improve antibiotic choice and clinical efficacy of treatments.

## **METHODS**

### Strains, media, and antibiotics

Lab strain *Escherichia coli* (MG1655) and a barcoded, clinical isolate *Escherichia coli* (PbEc)<sup>5</sup> were routinely cultured in lysogeny broth (LB) medium (RPI) aerobically (shaking at 230 rpm) at 37°C. When applicable, growth was determined by spectrometry (OD<sub>600</sub>), and survival was determined by enumeration of cultured colony forming units (CFU) on LB agar plates (RPI). Routinely, bacteria were collected and saved as a glycerol stock by combining 500 μL of bacteria culture with 500 μL 50% glycerol. Concentrated stocks of antibiotics levofloxacin (Alfa Aesar) and cefepime (Apotex) were prepared in

water and frozen for single use. Amikacin sulfate (Heritage) was diluted as needed from purchased liquid stock.

### Colony forming unit enumeration

Multiple assays relied on the enumeration of colony forming units. To perform these measurements, each well of 96 well plates was filled with 180  $\mu$ L of phosphate buffer saline (PBS, Sigma) solution. 20  $\mu$ L samples of cultures were then serially diluted (1:10) across the rows of 96 well plate up to a 10<sup>-6</sup> dilution. 20  $\mu$ L of each dilution was plated on LB agar plates in lines, and the plates were incubated overnight (37°C). The following day, individually colonies were counted from the plated dilutions with the maximum countable colonies. When necessary, cultures or aliquots were centrifuged and washed with PBS to remove antibiotic prior to diluting and plating.

### Evolution Assays

The evolution assay developed and used here was repeated daily beginning with a 1:10 dilution of overnight cultures into 10 mL of antibiotic-free LB media. Diluted cultures were grown for 1 hour. Prior to treatment, a 20  $\mu$ L sample was added to the 96 well plates prepared for CFU enumeration. The remaining culture was dosed with antibiotic and returned to shaking incubation. Diluting and plating related to CFU enumeration was performed during the incubation period. After the necessary incubation time (1 hour for levofloxacin and amikacin; 2 hours for cefepime), bacteria were pelleted by centrifugation (6000g, 5 minutes) and washed twice with PBS to remove the antibiotic. The cleaned pellets were resuspended with the equivalent volume of antibiotic-free LB media, and a post-treatment 20 $\mu$ L sample of the culture was collected for CFU enumeration. Cultures were promptly returned to shaking and incubation for overnight growth. The protocol was repeated daily until an increased sustained survival was observed. Percent survival was calculated by dividing post-treatment CFU counts by pre-treatment CFU counts. Sequential antibiotic treatments immediately followed the previous antibiotic treatment.

For the conventional laboratory evolution protocol, overnight cultures were diluted in antibiotic-free LB media (1:100). Antibiotic was serially diluted (1:2) across 5 mL LB media in 15 mL conical tubes to prepare a range of concentrations surrounding a predetermined MIC (MIC/4, MIC/2, MIC, 2xMIC, 4xMIC). Parental strain bacteria from the overnight growth were added (1:500) to tubes containing antibiotic and then grown aerobically overnight as described previously. The following day, the tube with the highest antibiotic concentration that allowed for robust growth was used to inoculate (1:500) freshly prepared conical tubes with an increased range of antibiotic concentrations relative to the prior day, centered around the passaged concentration (e.g., MIC/2, MIC, 2xMIC, 4xMIC, 8xMIC). This was repeated daily.

### Resistance Determination

In 96 well plates, twofold dilutions series of antibiotics were prepared in 100  $\mu$ L of LB media. Then, 100  $\mu$ L of diluted bacteria cultures ( $OD_{600}$ : 0.01) was added. Each plate included “Media Only” wells to measure background OD signal and “Cells Only” wells to assess maximum growth in the absence of antibiotic. Plates were incubated overnight at 37°C, shaking at 400 rpm, in a humidified (80%) incubator (Infors HT). Following incubation,  $OD_{600}$  was measured (Biotek Epoch2 plate reader), and raw OD values were exported and processed using a custom Python script.

First, a global or plate-specific median background was computed from the “Media Only” wells. This median value was subtracted from the raw data to correct for background signal. Next, each strain–antibiotic dataset was normalized by dividing the background-corrected OD values by the median OD of

its corresponding “Cells Only” wells, yielding fractional growth that ranged from near 0 (complete inhibition) to 1 (no inhibition). Using these normalized data, a two-parameter logistic (2PL) curve was fit to each strain–antibiotic combination. Specifically, the present function was employed to model growth

$$y(x) = \frac{1}{1 + \left(\frac{x}{IC_{50}}\right)^h}$$

where x is the antibiotic concentration, IC<sub>50</sub> is the concentration at which growth is half the no-antibiotic control, and h is the Hill slope reflecting the steepness of the inhibition curve. Experiments were conducted with technical triplicates across 12 antibiotic concentrations, ensuring sufficient data points across multiple conditions for robust curve fitting.

Parameter optimization was performed via SciPy’s least\_squares routine with a robust “dogbox” algorithm and “soft\_11” loss, which reduces sensitivity to outliers. The minimum inhibitory concentration (MIC) was then defined as the concentration at which growth reached 5% of the no-drug control (i.e., 95% inhibition). This value was obtained by numerically solving the fitted 2PL function at y=0.05. To quantify uncertainty in IC<sub>50</sub> and MIC estimates, a bootstrap analysis was performed by resampling each dose-response dataset 1,000 times with replacement and re-fitting the curve. The 2.5<sup>th</sup> and 97.5<sup>th</sup> percentiles of these bootstrap distributions defined 95% confidence intervals, providing robust estimates of parameter variability. When the model-predicted IC<sub>50</sub> or MIC exceeded the maximum tested antibiotic concentration, an “insufficient drug” flag was assigned, indicating that the true inhibitory concentration likely lay beyond the tested range, and excluded from further analysis.

### Statistical Analysis

Statistical analyses of MIC data were performed using Python (v3.10) with the `scipy.stats` package. Means and standard deviations of individual cultures within cohorts were calculated. Student’s t-test was used, assuming a normal distribution, to compare the means of relevant groups, treated vs parent and among segments of the sequential antibiotic treatments. Results are reported as mean ± standard deviation with their corresponding p-values. Significance p-value thresholds were noted with asterisks for p<0.05 (\*), p<0.01 (\*\*), p<0.001 (\*\*\*)<sup>\*\*\*</sup>, and p<0.0001(\*\*\*\*).

### Minimum duration of killing (MDK) assay

Overnight *E. coli* cultures were diluted 1:10 in antibiotic-free LB media and grown aerobically for 1 hour. Initial CFUs were measured as described previously. The cultures were then exposed to 129 µg/mL of cefepime for 7 hours. At hours 1, 2, 3, 5, and 7, 500 µL aliquots were collected in 1.5 mL microfuge tubes, centrifuged, and washed twice with PBS to remove the antibiotic. Pellets were resuspended in 500 µL PBS. At hours 5 and 7, final pellets were resuspended in 50 µL PBS, 20 µL of which was plated and 20µL was diluted further, to increase the limits of detection. CFUs were enumerated, and survivor fraction was calculated by dividing the ongoing counts by the initial CFU measurement. Results were reported as median ± median absolute deviation.

### Bacterial population sequencing

Bacteria cell pellets of antibiotic-evolved, passaged untreated control, and parental cultures were prepared from overnight cultures and sent to Seqcenter (Pittsburgh, PA) for DNA extraction (ZymoBIOMICS) and whole genome sequencing (Illumina). Samples were sequences using 150 base pair paired-end reads. For evolved cultures, approximately 2 giga base pairs of data per sample was received yielding coverage of

least 100x throughout the genome. Sequencing data was processed using breseq (Barrick lab), comparing reads to a MG1655 reference genome<sup>76</sup>. Alleles present in the passaged, untreated controls were tracked but were removed from the dataset of evolved populations. Likewise, alleles present in the parental strain relative to the reference genome were subtracted. Remaining mutations were filtered to include only those which exceeded 10% at any timepoint and these alleles were traced across timepoints.

### Oligo recombineering

Chromosomal mutations were made using oligo recombineering, and gene deletions were made using oligo recombineering followed by Bxb-1-Integrase-Targeting (ORBIT). These methods each incorporate mutations encoded on transformed oligonucleotides through homologous recombination during DNA replication, and require elements encoded on a helper plasmid<sup>51</sup>. Parental MG1655 bacteria were made electrocompetent and then transformed with the pHelper\_Ec1\_V1\_gentR (pHelper-V1) for oligo recombineering or with pHelper\_noMutL\_V2\_gentR (pHelper-V2) for ORBIT. Selection was made possible by gentamicin. pHelper-V1 expresses single stranded DNA annealing proteins (SSAP), CspRecT, and a dominant negative MutL, which improves editing efficiency by suppressing mismatch repair<sup>77</sup>. Sucrose counterselection is made possible by *sacB* gene encoded on the plasmid. The expression is driven by the induction of the XylS/m-toluic acid system. pHelper-V2 differs in that it does not include the dominant negative MutL. Transformed bacteria were induced with toluic acid for 1 hour prior to storage at -80°C.

For simple oligo recombineering, 90-nucleotide long oligonucleotides were designed with the desired mutations at the center flanked by homology regions within the gene, and each was ordered from Integrated DNA Technologies (IDT) (Table1). Oligonucleotides were prepared and diluted to 25nM in water. 50 µL of MG1655-pHelper-V1 was mixed with 2 µL of diluted oligonucleotide, electroporated (1.8mV), and recovered in LB media for 1 hour at 37°C. Recovered bacteria were streaked on LB agar for single colonies and incubated overnight at 37°C.

Individual colonies were picked into 100 µL PBS in 96 well plates for screening by polymerase chain reaction (PCR). Throughout screening, colonies were routinely substreaked on LB-sucrose (7.5%) plates to drive the removal of the pHelper-V1 plasmid. Plasmid loss was confirmed by plating on LB-gentamycin (15 µg/mL) plates.

### Preparation of electrocompetent cells

MG1655 cultures were made electrocompetent prior to transformations with plasmids pHelper-V1 and pHelper-V2, and subsequently MG1655-pHeper-V1 and MG1655-pHelper-V2 were made electrocompetent prior to transformations with oligonucleotides. Each approach varied slightly.

Beginning with plasmid transformations, filtered water was aliquoted in 50 mL conical tubes and refrigerated overnight. MG1655 was cultured overnight in 10 mL LB media. The following day, a 1:100 dilution of the overnight was performed into a fresh 10 mL LB and grown for 2 hours. During this time, the water aliquots, empty 15 mL conical tubes, and microfuge tubes were placed on ice. After 2 hours of growth, the culture was split into two, 15 mL tubes. These cultures were centrifuged at 4000g, 2°C, for 10 minutes. The pellets were washed twice with 10 mL of cold water. The final supernatant was fully removed by pipetting. Pellets were then resuspended in 1 mL of cold water, combined, and then split into 2 microfuge tubes. The microfuge tubes were centrifuged for 10 minutes, and each pellet was resuspended in 100 µL of cold water. In separate tubes, 100 µL of the culture was combined with 20 ng of either plasmid and each was electroporated (2.5 kV). Immediately, 1 mL of prewarmed recovery media (NEB) was added and moved to a 15 mL conical tube where it recovered for 1 hour at 37°C in the shaking

incubator. Following its recovery, 200  $\mu$ L of each culture was plated on LB agar plates containing 15  $\mu$ g/mL gentamycin for positive selection of transformants. A non-transformed culture was used as a control. After overnight incubation, single colonies were picked and grown overnight in liquid culture with gentamycin (15  $\mu$ g/mL).

The following day, the cultures, transformed MG1655-pHelper-V1 and MG1655-pHelper-V2 were induced and made competent again. Filtered water and 10% glycerol had been refrigerated overnight. From the overnight cultures, a 1:1000 dilution was made into 200 mL of LB with gentamycin and grown for 3-4 hours to ~ 0.3 OD. While growing, reagents and tubes were placed in ice. When the cultures reached 0.3 OD, the cultures were induced with 1 mM toluic acid (added from a 1000x stock solution) and incubated for 30 minutes. Following incubation, the cultures were removed and placed in an ice bath with occasional swirling to stop their growth. Then 50 mL aliquots of the cultures were transferred to iced conical tubes. These were centrifuged at 5000g for 10 minutes at 2°C. The supernatant was poured off, and pellets were resuspended with 45 mL cold water. Resuspended pellets were centrifuged, and pellets were resuspended with 10% glycerol. This was repeated twice more, but the final pellets were resuspended in the residual glycerol. Cultures of the same strain were pooled and then aliquoted (100  $\mu$ L) into small microfuge tubes. These were chilled on dry ice for 5-10 minutes before being stored at -80°C. These resulting stocks were competent and induced to allow for the transformation and incorporation of targeting oligonucleotides.

### Polymerase chain reaction and SDS page

Cultures transformed with oligonucleotides were plated on non-selective plates, and thus colonies required screening by PCR and then confirmation by Sanger Sequencing (Eurofins).

For each mutant strain prepared, full-length and mutant-specific PCR primers were designed (Table 2). The mutant-specific primers relied on the small differences in sequences and were paired with the full-length primer in the opposite direction. PCR reactions were performed using GoTaq polymerase (Promega), the appropriate primer set, water, and a 1  $\mu$ L inoculation of the colony-PBS suspension. Prior to screening, the melting temperatures for reactions using mutant specific primers were optimized by gradient PCR of parent strain and a pool of presumptive mutant colonies. Then, batches of individual colonies were screened by mutant-specific PCR. Mutant PCR reaction products were routinely run on 1% agarose gels with ethidium bromide and imaged under ultraviolet light (Syngene G:BOX Chemi XT4 with GeneSys software). Positive colonies were then PCR amplified using full-length primer pairs. These full-length PCR products were cleaned (Nucleospin Gel and PCR cleanup kit) and submitted for Sanger sequencing (Eurofins).

Analysis of the sequencing results often revealed mixed colonies with peaks representing mutant and wild-type nucleotides. When this occurred, positive colonies were substreaked (LB-sucrose), and rescreened. After several iterations, Sanger sequencing results were pure, and the mutational status was confirmed by sequencing further subclones for purity. For the larger mutations made by oligo recombineering, the efficiency was lower and required a pooling approach to minimize reagent use and increase throughput. When mutants were confirmed and purity achieved, single colonies were picked and grown in LB overnight and then saved as stocks in 25% glycerol.

### Bacterial growth assay

Strains were cultured overnight from glycerol stocks in 10 mL LB media. The following day, a 96 well plate was prepared with 100  $\mu$ L LB media in each well. Overnight cultures were diluted in fresh media to an OD<sub>600</sub> of 0.1. To media-only wells, an additional 100  $\mu$ L LB media was added. To culture wells, with

six replicates of each strain, 100  $\mu$ L of diluted culture was added. The plate was promptly incubated in Bitek Epoch2 plate reader and grown for 20 hours at 37°C with shaking. Every 2 minutes, OD measurements were made. Growth curves were analyzed using a custom Python script. OD readings were first filtered to values between 0.02 and 0.08 to capture the log growth phase. Linear regressions were performed on the log transformed OD values within this range as a function of time. The resulting slope was converted to a natural log-based growth rate. Doubling time was then calculated using the formula

$$\frac{\ln(2)}{\text{growth rate}}$$

and reported in minutes. The `scipy.stats` module was used to calculate means, standard deviations, and to perform t-tests of doubling times.

### Cell fixation for single cell RNA sequencing

Overnight cultures of strains were inoculated (100 $\mu$ L in 10mL) from frozen stocks, avoiding population bottlenecking. Cultures were diluted to 1 OD, and 1 mL of culture was fixed with 67 $\mu$ L of paraformaldehyde through a 30 minute incubation. Paraformaldehyde was removed by centrifugation (5 min, 6000 rcf). Pellet was resuspended with 1 mL of 0.2x SSC Buffer (Invitrogen). Buffer was removed by centrifugation, the pellet was resuspended in 350  $\mu$ L of MAAM (4 parts methanol, 1 part acetic acid), and briefly stored at -20°C.

### Single cell RNA sequencing

Fixed cells were processed using standard ProBac-seq protocols as follows: 100  $\mu$ l of cells in MAAM solution were centrifuged at 6000 rcf and washed 3 times in 300  $\mu$ l PBS solution. After PBS washes cells were permeabilized by incubation for 30 minutes with 250 units of lysozyme (ReadyLyse, LGC BioSearch) in 100 $\mu$ l PBS. Cells were centrifuged again at 6000 rcf and washed with 300 $\mu$ l 1x PBS with 0.1% tween solution. Cells were again centrifuged and washed in PBS to remove the detergent and resuspended in Probe Binding Buffer (100  $\mu$ l of probe binding buffer consisting of 5  $\times$  SSC, 30% formamide, 9 mM citric acid at pH 6.0, 0.1% Tween 20, 50  $\mu$ g/ml heparin and 10% low molecular weight dextran sulfate). Cells were incubated for 30 minutes at 50°C before 25  $\mu$ l of probes were added at a concentration of 1,200 ng/ $\mu$ l, and the mixture was left to incubate overnight at 50°C with shaking at 300 RPM. Following incubation cells were washed 7 times in probe-wash solution at 50°C (5  $\times$  SSC, 30% formamide, 9 mM citric acid pH 6.0, 0.1% Tween 20 and 50  $\mu$ g/ml heparin) and finally washed twice in room temperature PBS.

Single-cell microfluidic encapsulation was done using a 10X Genomics chip-G and a Chromium Controller with the Chromium Single Cell 3' Reagents Kit (v3 chemistry) as described by 10X Genomics using a protocol modified to achieve bacterial scRNA-seq described previously <sup>78,79</sup>. For encapsulation a master mix containing the following reagents was prepared: 33  $\mu$ l of 4X ddPCR Multiplex Supermix (BioRad), 4  $\mu$ l of in-drop PCR primer (10  $\mu$ M), 2.4  $\mu$ l additive A (10X Genomics) and 26.8  $\mu$ l dH<sub>2</sub>O. Prepared cell samples were diluted to 1,000 cells  $\mu$ l<sup>-1</sup> and loaded as a total of 16,000 cells per condition to achieve a targeted cell recovery of 10,000 cells. After encapsulation each sample was transferred to an individual PCR tube and cycled 6 times using the following thermocycler program: 94 °C for 5 min (before cycling), 94 °C for 30 s followed by 50 °C for 30 s then 65 °C for 30 s for 6 cycles and a final hold at 12 °C.

Libraries for NGS sequencing were completed using two additional PCR reactions as detailed previously<sup>78,79</sup> and sequenced using an Element AVITI 150 cycle kit using paired end sequencing of 8 bp for the i7 index, 28bp for Read 1 and the remaining cycles for Read 2.

Reads were trimmed and the probe-based UMI was upended in place of the traditional 10X-bead provided UMI using cutadapt in order to allow for true molecular identification, as detailed previously<sup>78,79</sup>. Samples were mapped and aggregated using the 10X cellRanger pipeline. Analysis of single cell libraries was done using the R-based Seurat pipeline<sup>80</sup>. Standard parameters in Seurat were used for data normalization and to identify the variable features. Louvain clustering was used with resolution set to 0.7 using Seurat FindClusters function. We tested a range of resolutions from 0.5 to 1.5 and find that the main clustering features presented in the text remain across this range of clustering parameters. The Seurat function FindMarkers was used and a log-fold change cutoff of 0.5 chosen to highlight highly differential genes in the main-text volcano plots and a log-fold change cutoff of 0.25 for the supplementary volcano plots in the Supplementary Figures. The full output for all differentially expressed genes is shown in the DGE Supplementary Tables.

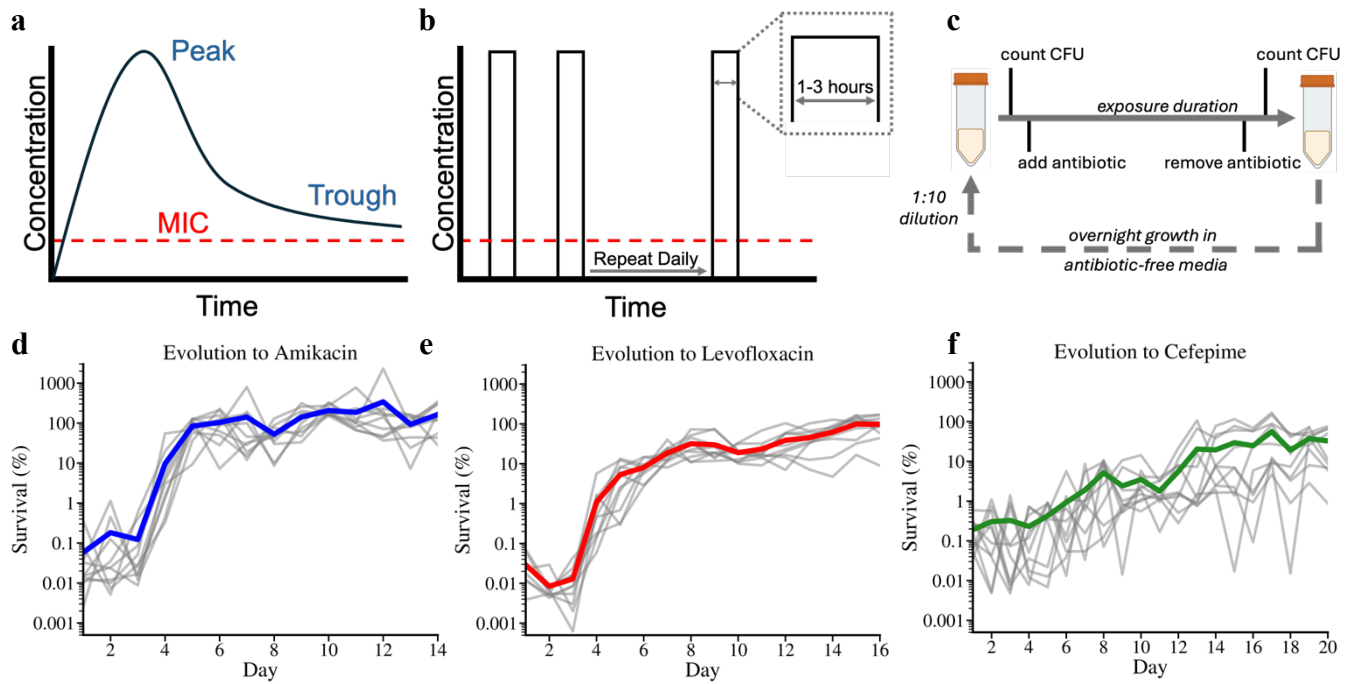


**Figure 1. Evolution protocol rationale, scheme, and survival outcomes of single antibiotic evolutions.** **a,** Illustration of the pharmacokinetics in a clinical antibiotic regimen with peak and trough antibiotic concentrations remaining above the minimum inhibitory concentration (MIC). **b,** Laboratory adaptation of clinical parameters for evolution experiments featuring daily antibiotic exposures at peak concentrations with adjustable exposure durations. **c,** Complete evolution protocol workflow. CFU counts are measured before and after antibiotic addition and removal, followed by overnight growth in antibiotic-free media and a 1:10 dilution after overnight growth. **d-f,** Survival trajectories of bacterial cultures evolved in the presence of amikacin, levofloxacin, and cefepime, respectively. Gray lines represent individual replicate cultures, while colored lines represent the mean survival over time for amikacin (blue), levofloxacin (red), cefepime (green).

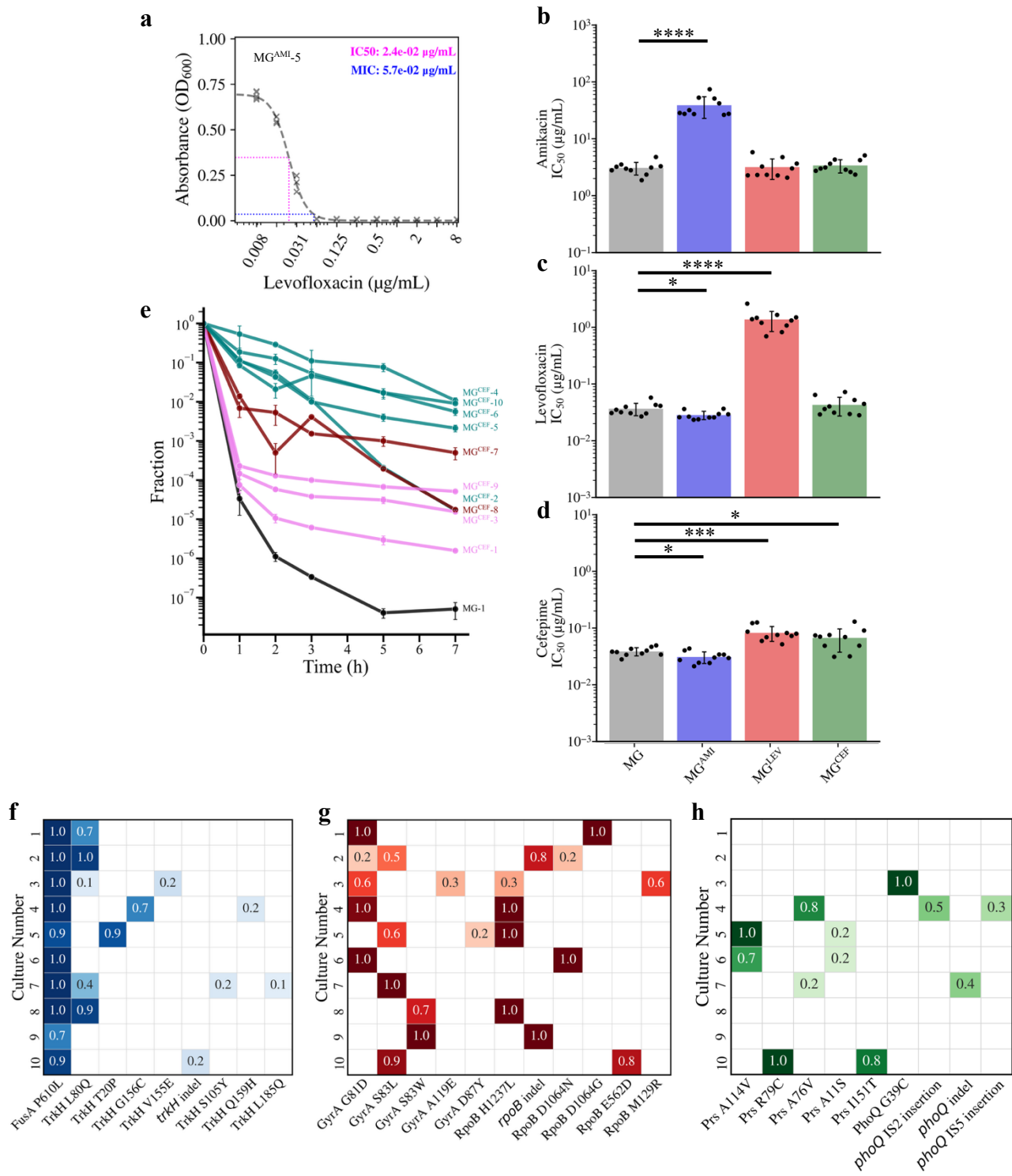


**Figure 2. Phenotypic and genotypic outcomes of evolutions to single antibiotics.** a, representative IC<sub>50</sub> and MIC determination from a dose-response curve. b-d, bar plots of IC<sub>50</sub> values in antibiotics amikacin, levofloxacin, and cefepime, respectively for parental and evolved cohorts (MG: gray; MG<sup>AMI</sup>: blue; MG<sup>CEF</sup>: green; MG<sup>LEV</sup>: red). Bar height corresponds to the mean IC<sub>50</sub>, and error bars reflect the standard deviation. Individual IC<sub>50</sub> values for replicate cultures are shown as dots. Statistical significance (p-value, student's t-test) is denoted by asterisk (\* < 0.05; \*\* < 0.01, \*\*\* < 0.001, \*\*\*\* < 0.0001), a convention used in subsequent figures. e, MDK assay for cefepime-evolved cultures (MG<sup>CEF</sup>) showing the median survivor fraction plotted over time, with error bars representing the median absolute deviation (MAD). Line colors differentiate the parental strain (MG: black) and evolved cultures that are characteristically tolerant (teal), persistent (pink), or of an intermediate phenotype (maroon). f-h, heatmaps of selected mutations and their frequencies among individual cultures: f, MG<sup>AMI</sup> (blue); g, MG<sup>LEV</sup> (red); g, MG<sup>CEF</sup> (green).

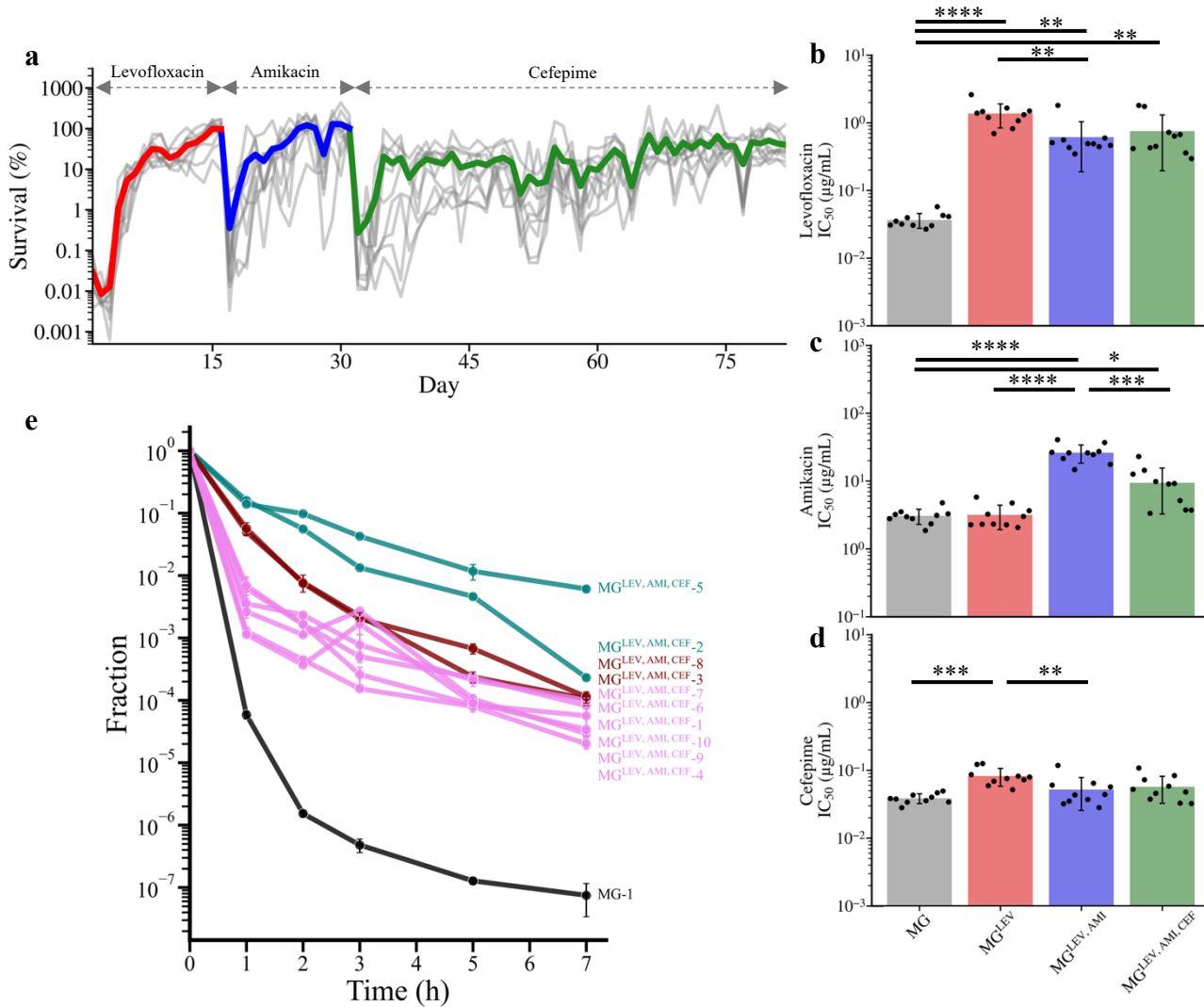


**Figure 3. Survival and phenotypic outcomes of sequential antibiotic treatment.** a, survival trajectories of bacteria cultures sequentially evolved in the presence of levofloxacin (red), amikacin (blue), and cefepime (green). Gray lines represent individual cultures, and colored lines indicate the mean survival through the respective antibiotic: levofloxacin (red), amikacin (blue), cefepime (green). b-d, bar plots of  $IC_{50}$  values in antibiotics levofloxacin, amikacin, and cefepime, respectively, for parental and evolved cohorts (MG: gray; MG<sup>LEV</sup>: red; MG<sup>LEV,AMI</sup>: blue; MG<sup>LEV,AMI,CEF</sup>: green). Bar height corresponds to the mean  $IC_{50}$ , and error bars reflect the standard deviation. Individual  $IC_{50}$  values for replicate cultures are shown as dots. e, MDK assay for sequentially evolved cultures (MG<sup>LEV,AMI,CEF</sup>) showing the median survivor fraction plotted over time, with error bars representing the median absolute deviation (MAD). Line colors differentiate the parental strain (MG: black) and evolved cultures that are characteristically tolerant (teal), persistent (pink), or of a mixed phenotype (maroon).

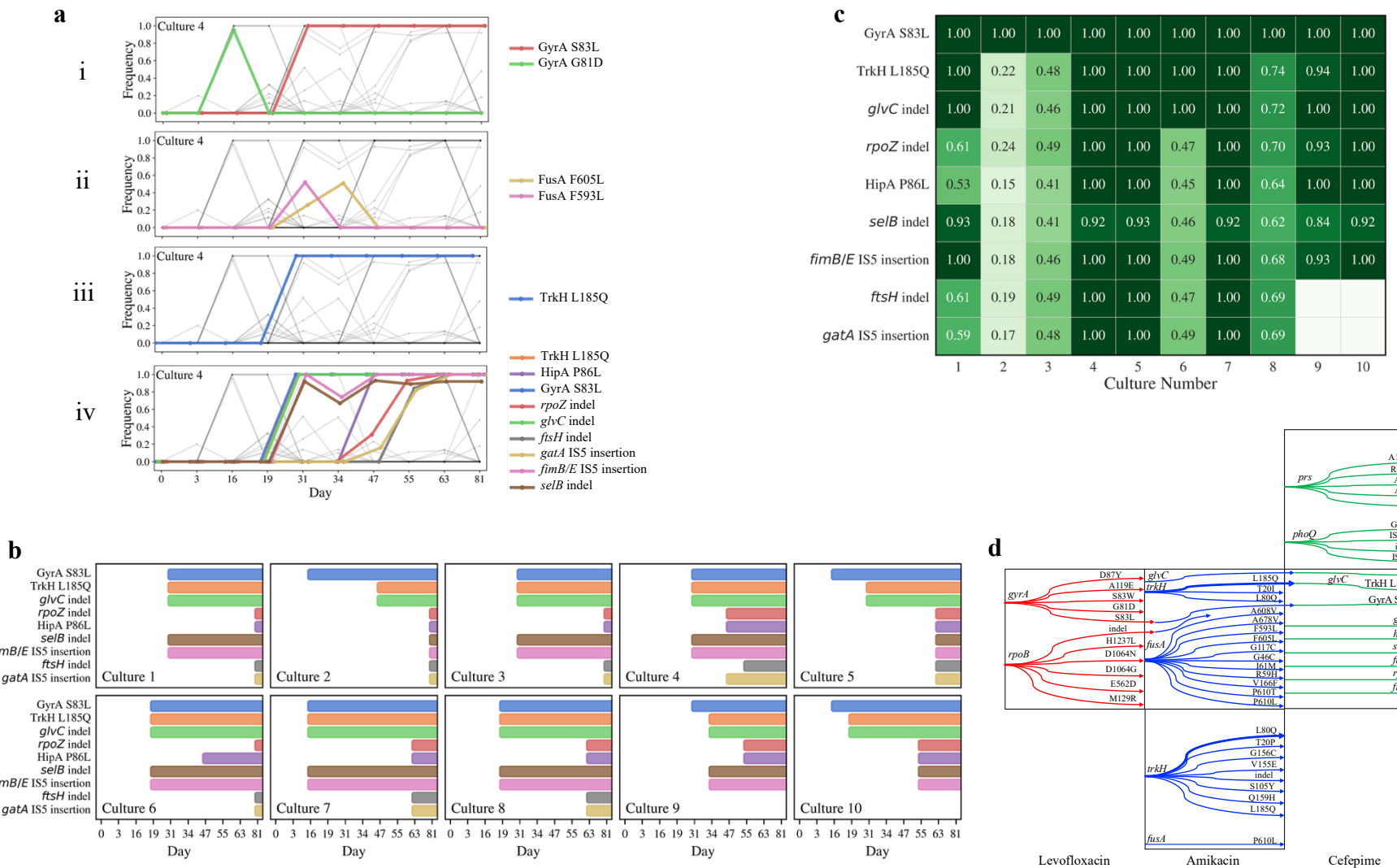


**Figure 4. Genotypic outcomes of sequential antibiotic evolution.** a, mutation trajectories in Culture 4 of *gyrA* (i), *fusA* (ii), *trkH* (iii) and within the convergent clade mutations (iv). b, emergence and cadence of clade mutations within individual cultures. c, heatmap of final frequencies of convergent clade mutations across replicate cultures. d, cartoon depicting the observed impact of single vs. sequential treatment context on divergent and convergent mutation trajectories (arrows) under the selection of levofloxacin (red) amikacin (blue) and cefepime (green). Arrows are noted with mutations.

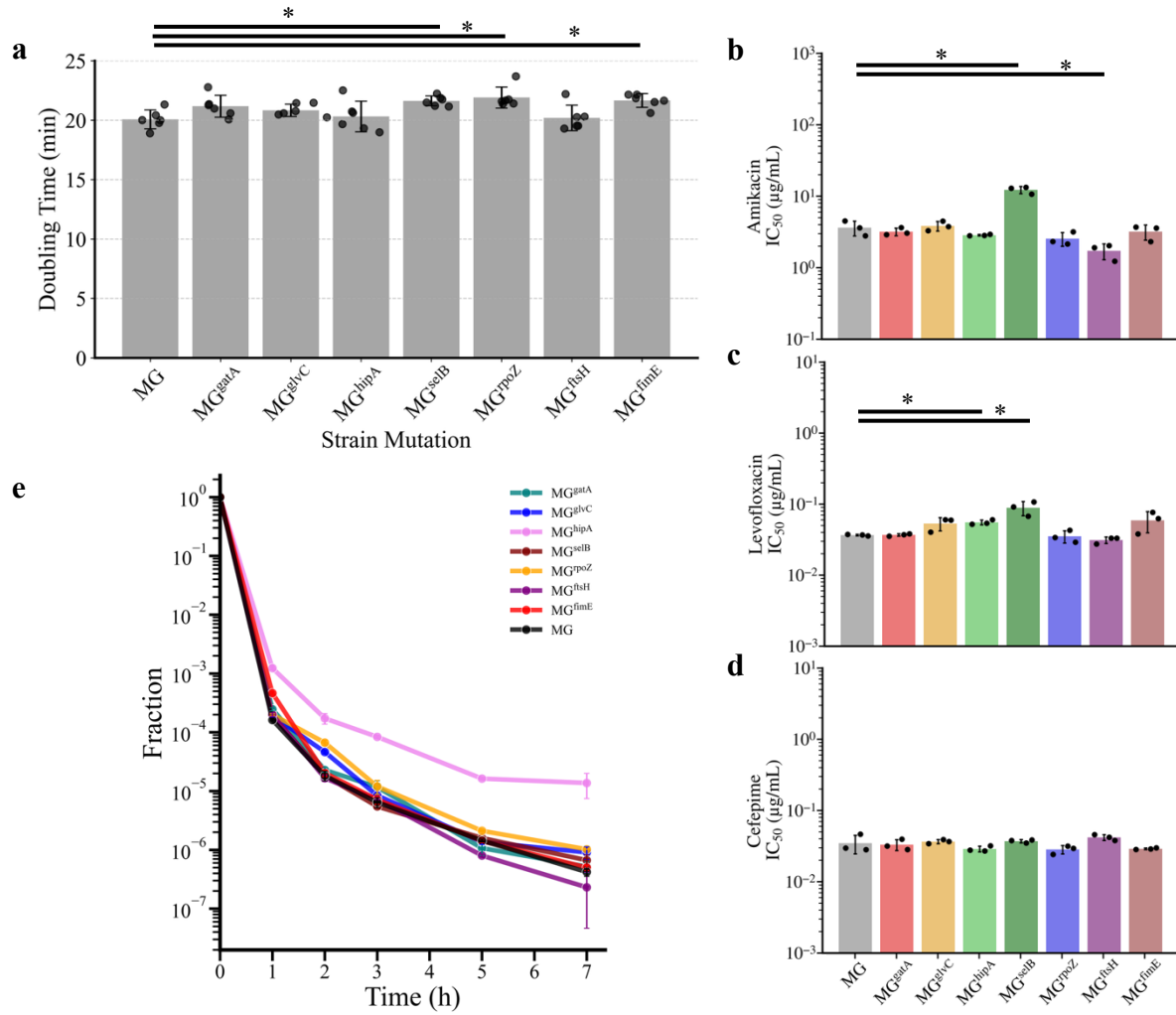


**Figure 5. Phenotypic effects of individual convergent clade mutations.**

a, barplot of doubling times of mutant and parent (MG) strains show mean values of six replicates (dots) with error bar indicating the standard deviation. b-c, IC<sub>50</sub> of individual mutants in each antibiotic, where bar height shows the mean value for three replicates (dots) and error bar indicates standard deviation. d, MDK of mutants with median survival plotted for three replicates and error bar is the median absolute deviation.

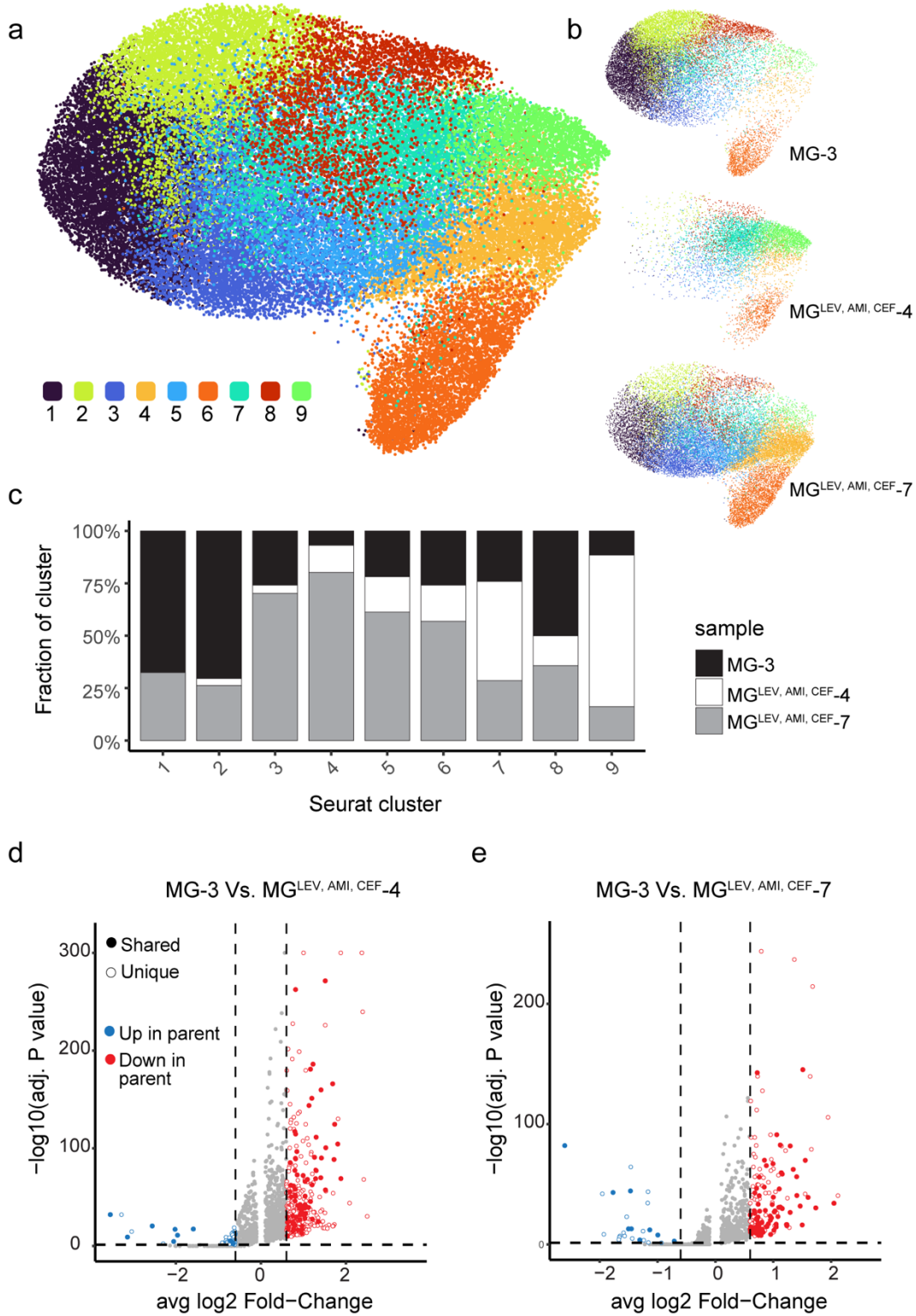
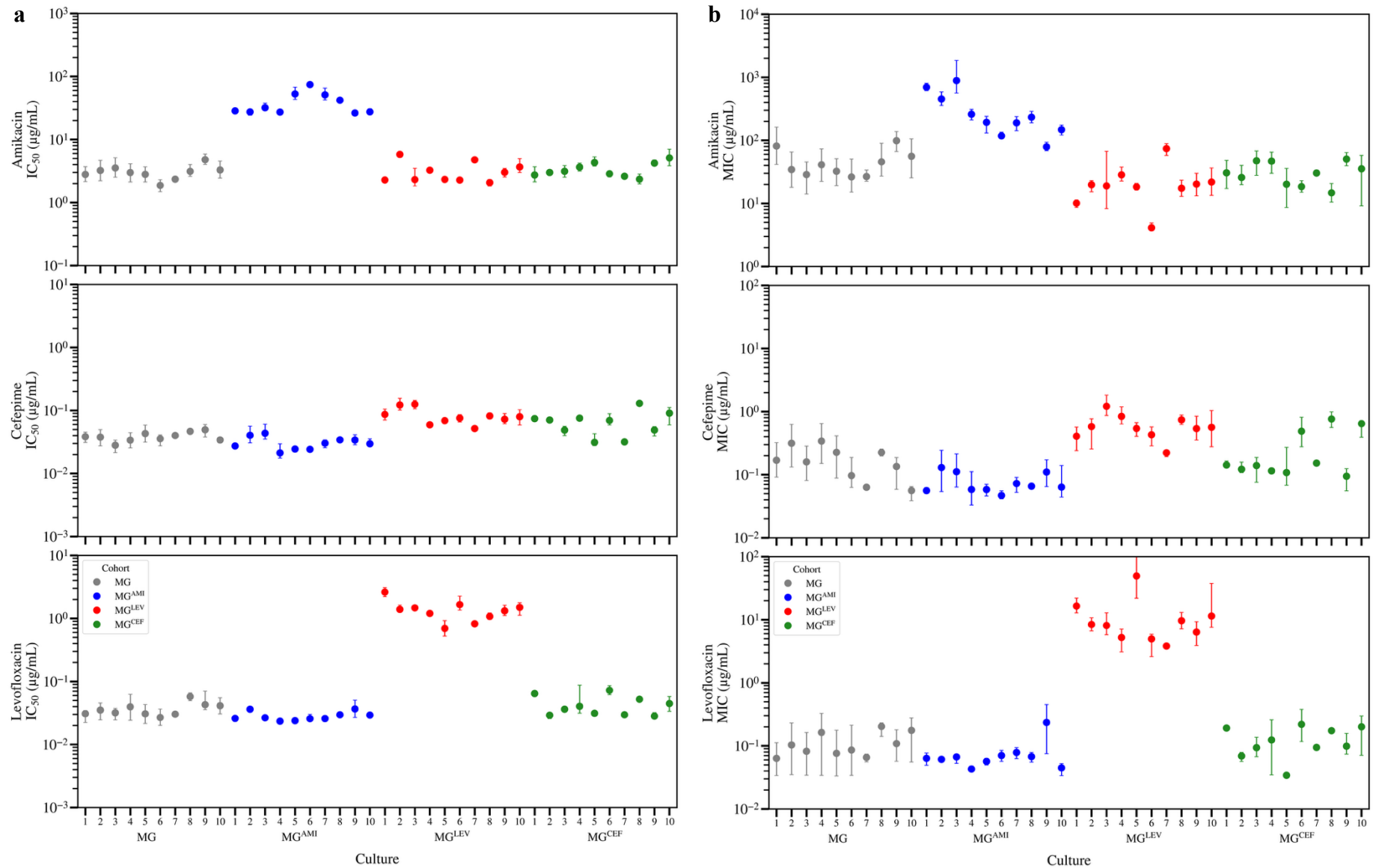
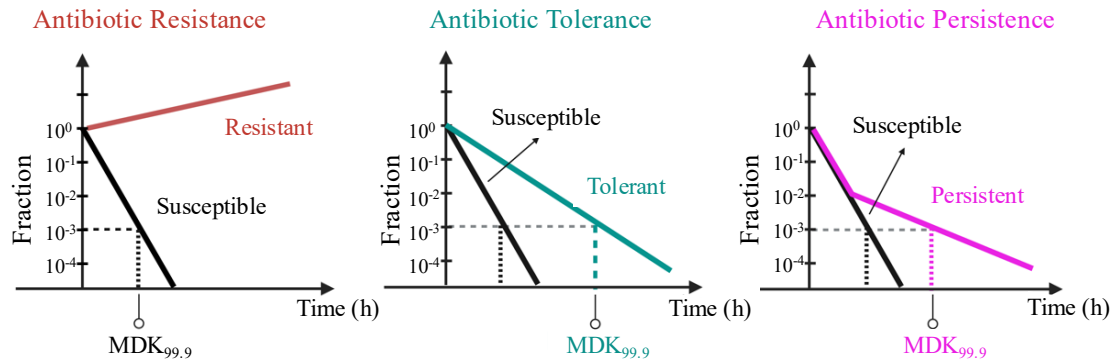


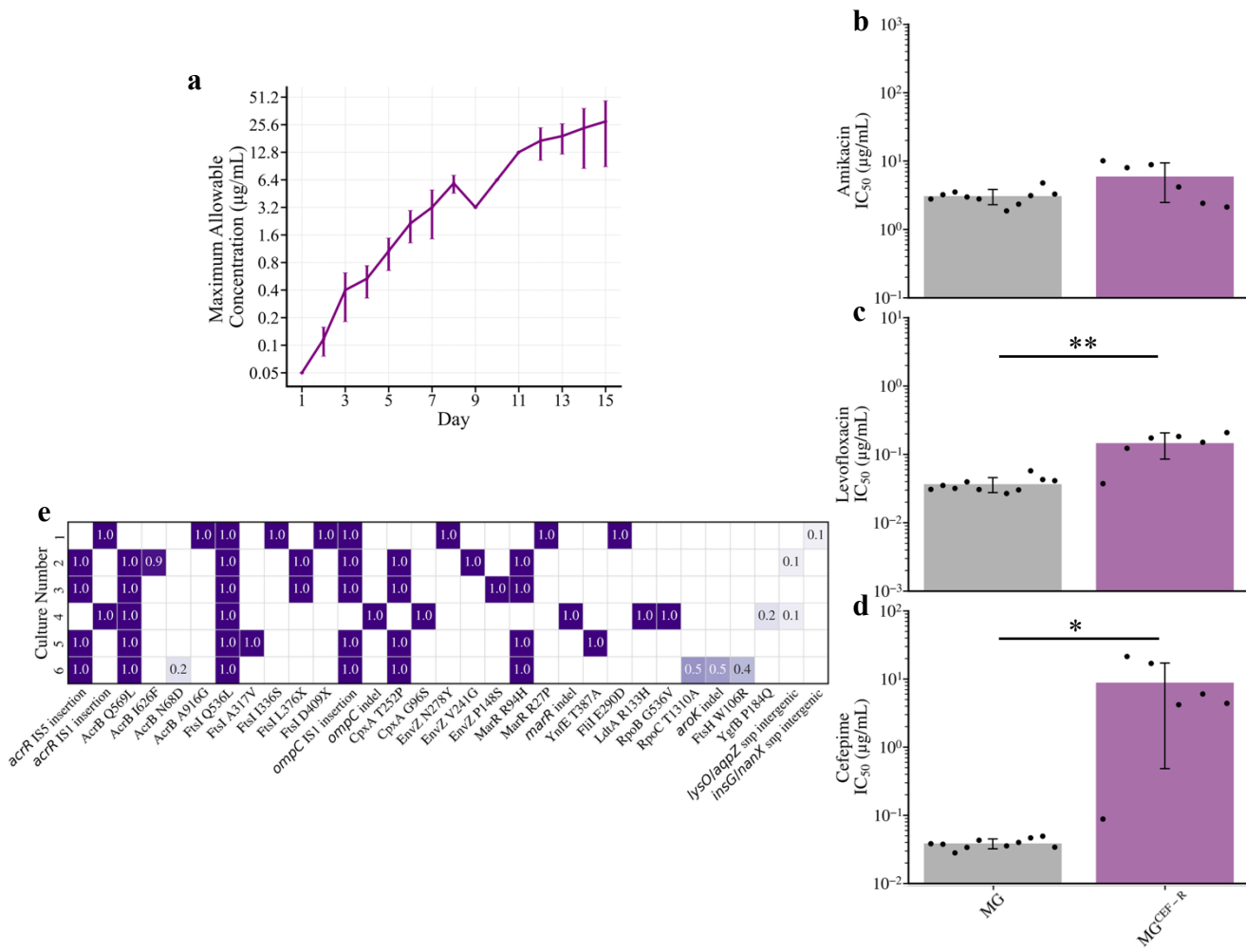
**Figure 6.** a, UMAP two-dimensional representation of the 9 cell clusters identified in the combined dataset of 48,883 cells. b, UMAP showing cells in either the parental culture (top) or evolved cohorts (middle and bottom). c, Stacked bar chart showing the percent community composition of each cell cluster. d,e, Volcano plot of genes expressed in the parent or MG<sup>LEV, AMI, CEF-4</sup> (d) and MG<sup>LEV, AMI, CEF-7</sup> (e). Genes shared between the two evolved strains are denoted by solid markers. Adjusted P values correspond to two-sided Wilcoxon rank-sum test with Bonferroni correction.



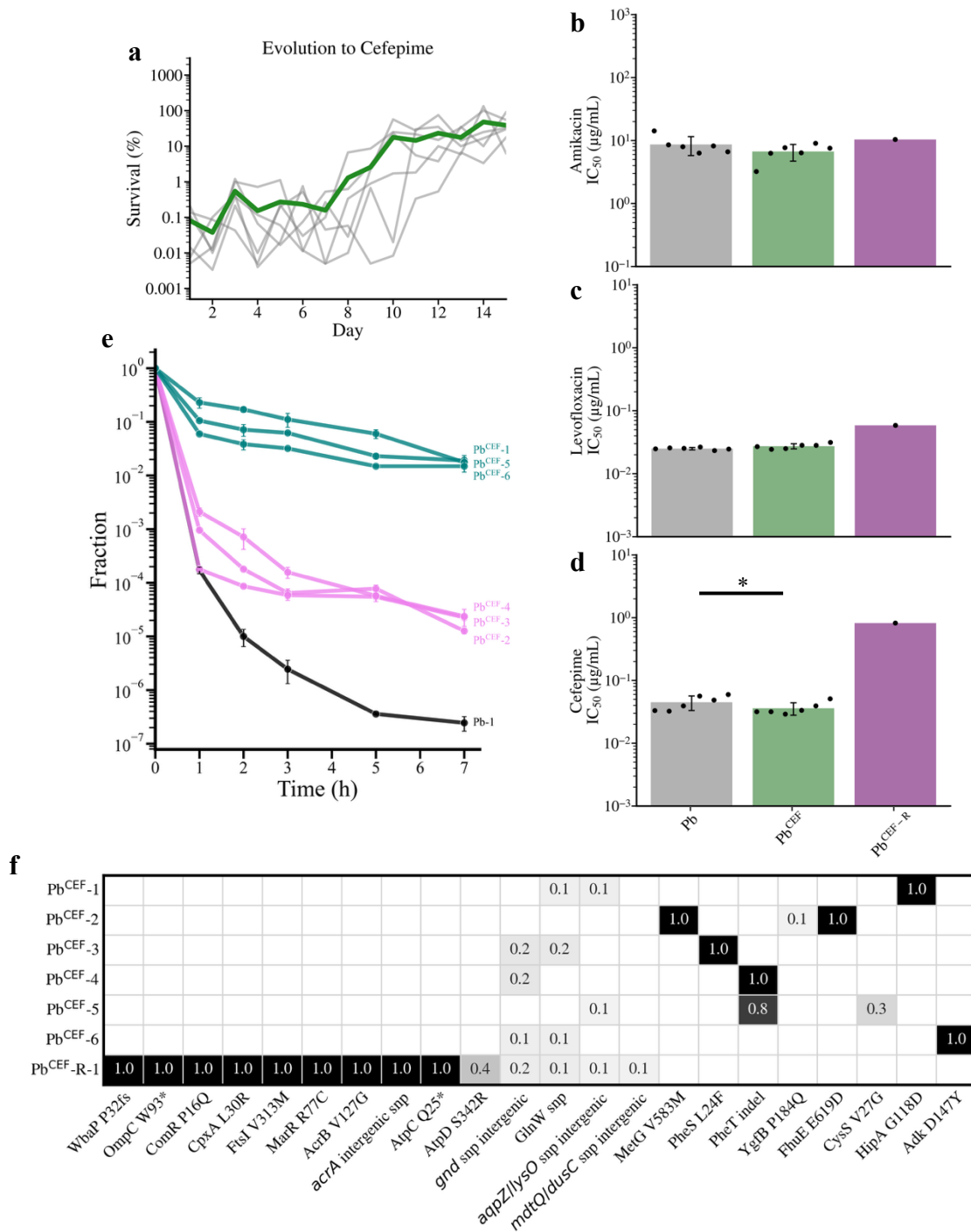
**Supplemental Figure 1. IC<sub>50</sub> and MIC values of individual evolved cultures.** a, Average IC<sub>50</sub> values (error bars: standard deviation) for individual cultures of parental strain (MG, gray) and cultures evolved in the presence of amikacin (MG<sup>AMI</sup>: blue), cefepime (MG<sup>CEF</sup>: green), and levofloxacin (MG<sup>LEV</sup>: red). b, Average MIC values (error bars: standard deviation) for individual cultures of parental strain (MG, gray) and cultures evolved in the presence of amikacin (MG<sup>AMI</sup>: blue), cefepime (MG<sup>CEF</sup>: green), and levofloxacin (MG<sup>LEV</sup>: red).



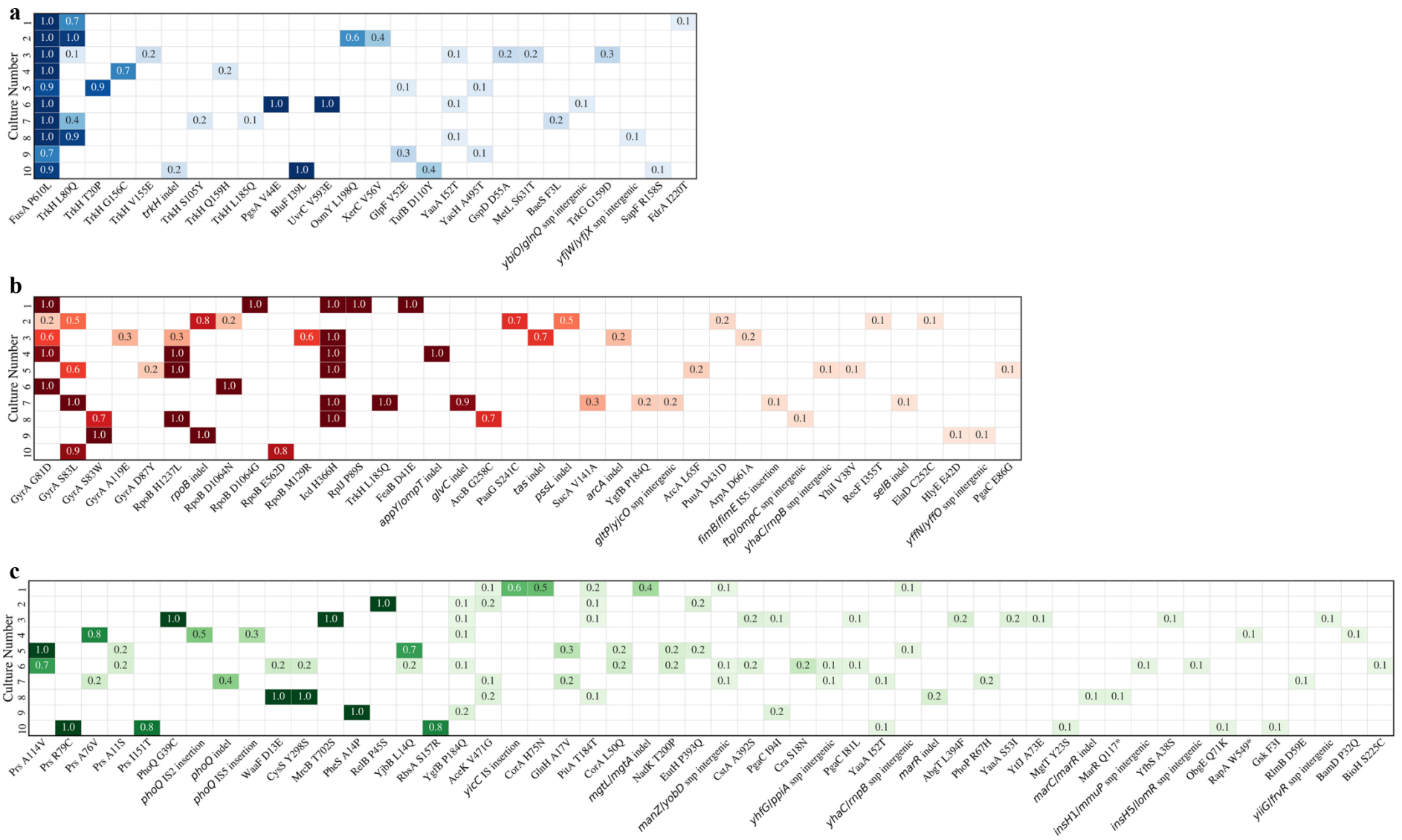
**Supplemental Figure 2. Differences among survival strategies in time kill assay.** Illustration of the MDK curves expected for bacteria which are resistant (red), tolerant (teal), persistent (pink), and susceptible (black). Differences include shifts in the minimum duration for killing 99.9% of bacteria ( $MDK_{99.9}$ ) and the biphasic nature of the MDK curve in persistent populations.



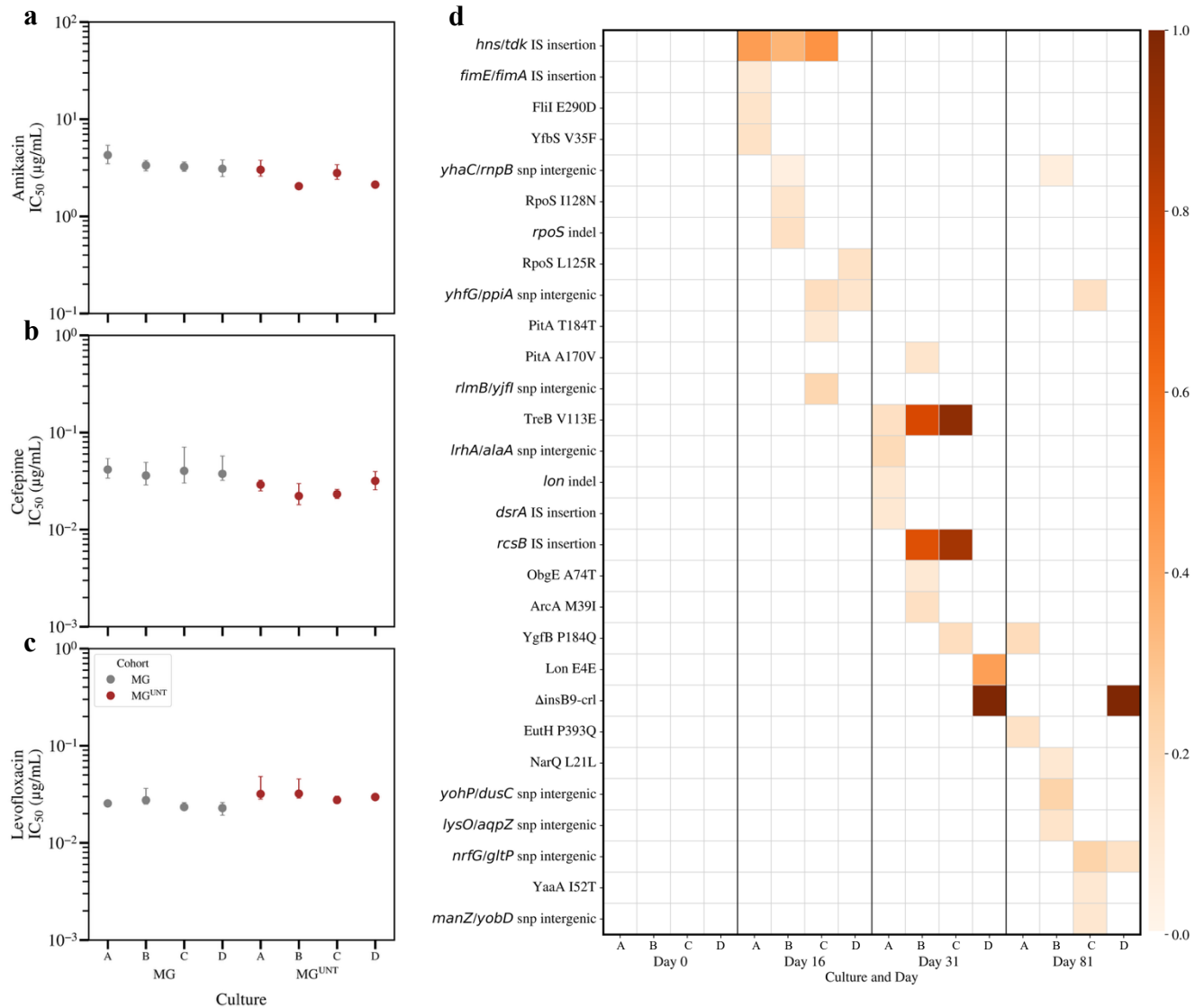
**Supplemental Figure 3. Phenotypic and genotypic outcome of cefepime resistance evolution protocol in lab strain.** a, Maximum allowable concentration for growth over time in conventional evolution in the presence of cefepime. Plotted line represents the mean concentration and error bars represent the standard deviation. b-d, bar plots of  $\text{IC}_{50}$  values in antibiotics amikacin, levofloxacin, and cefepime, respectively for parental and cefepime-resistance evolved cohorts (MG: gray; MG<sup>CEF-R</sup>: purple). Bar height corresponds to the mean  $\text{IC}_{50}$ , and error bars reflect the standard deviation. Individual  $\text{IC}_{50}$  values for replicate cultures are shown as dots. e, heatmap of selected mutations and their frequencies among individual cultures of MG<sup>CEF-R</sup>.



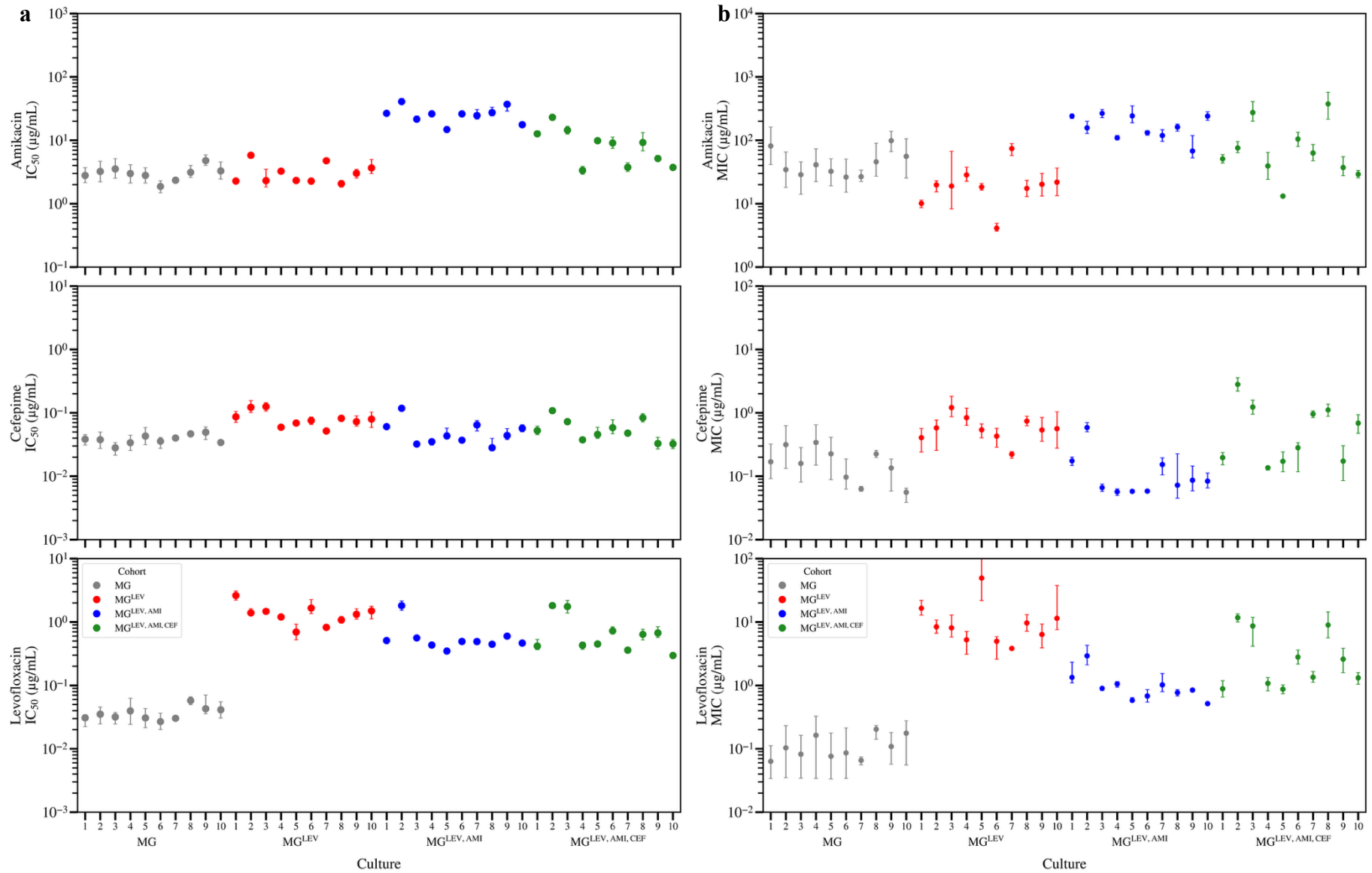
**Supplemental Figure 4. Phenotypic and genotypic outcomes of cefepime evolution in clinical strain.** a, Survival trajectories of clinical bacterial cultures evolved in the presence cefepime. Gray lines represent individual replicate cultures, and the mean survival is shown in green. b-d, bar plots of  $IC_{50}$  values in antibiotics amikacin, levofloxacin, and cefepime, respectively, for unevolved clinical strain (Pb: gray), cefepime-evolved clinical strain using our evolution protocol (Pb<sup>CEF</sup>: green) and cefepime-evolved clinical strain using the conventional evolution protocol (Pb<sup>CEF-R</sup>). height corresponds to the mean  $IC_{50}$ , and error bars reflect the standard deviation. Individual  $IC_{50}$  values for replicate cultures are shown as dots. e, MDK assay for cefepime-evolved clinical cultures in our evolution protocol (Pb<sup>CEF</sup>) showing the median survivor fraction plotted over time, with error bars representing the median absolute deviation (MAD). Line colors differentiate the parental strain (Pb: black) and evolved cultures that are characteristically tolerant (teal) and persistent (pink). f, heatmap of mutations and their frequencies among individual cultures of Pb<sup>CEF</sup> and Pb<sup>CEF-R</sup>.



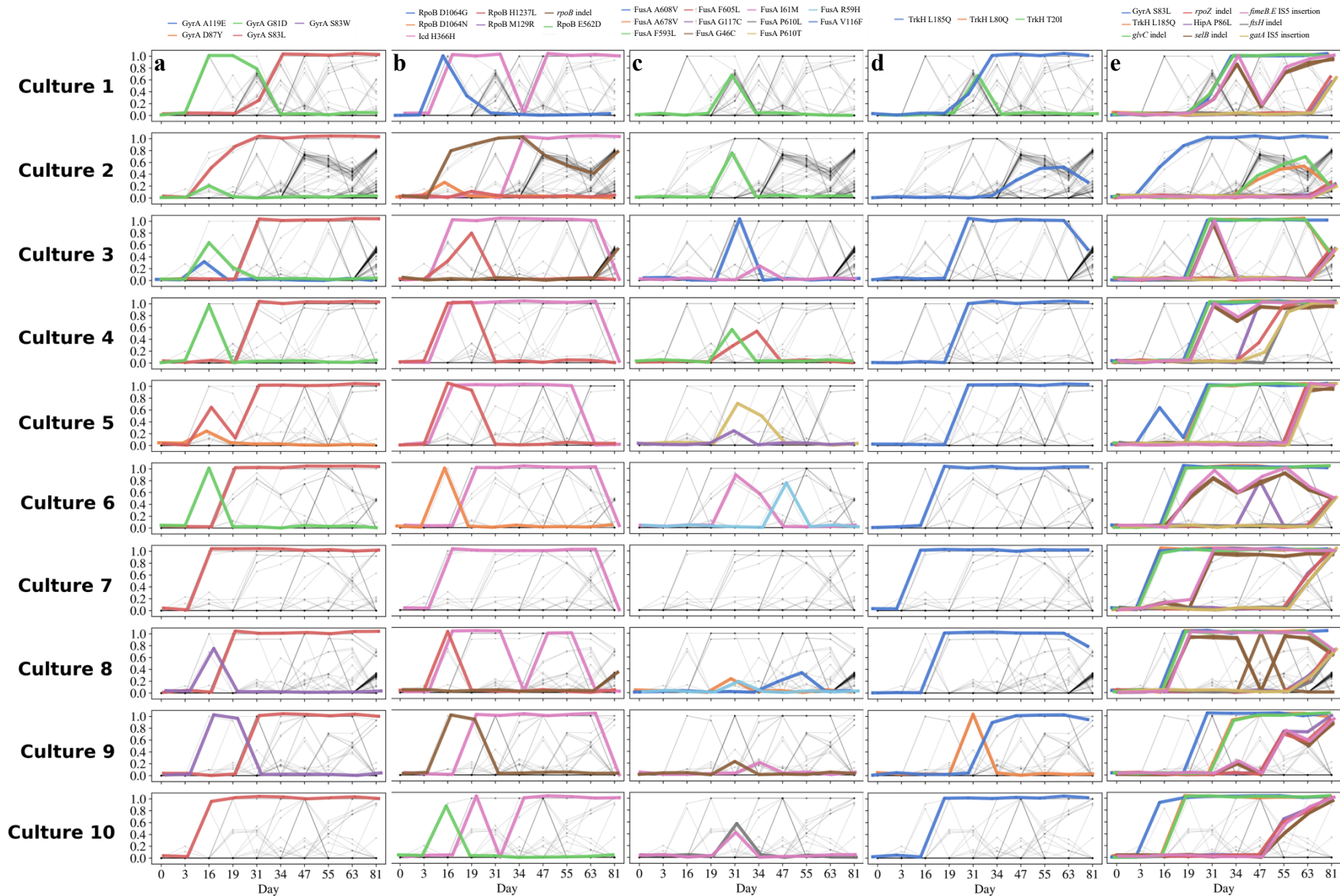
**Supplemental Figure 5. Extended genotypic outcomes of single antibiotic evolutions.** Heatmaps of extended mutations and their frequencies among individual cultures: a, MG<sup>AMI</sup> (blue); b, MG<sup>CEF</sup> (green); c, MG<sup>LEV</sup> (red).



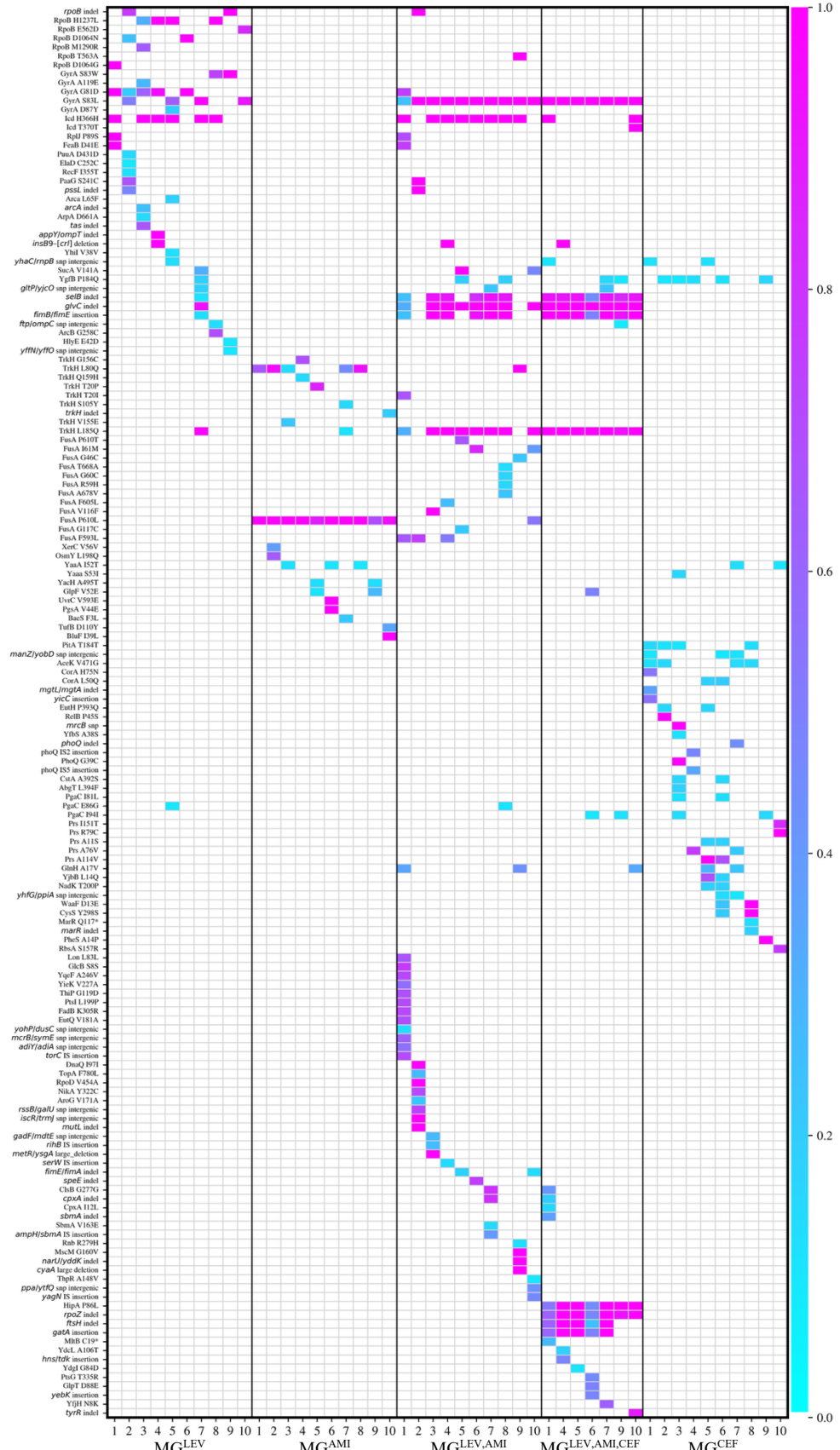
**Supplemental Figure 6. Phenotypic and genetic outcome following untreated passage of MG1655.** a-c, IC<sub>50</sub> values of parent and untreated, passages control populations in each antibiotic, amikacin (a), cefepime (b), levofloxacin (c). d, heatmap of mutational changes throughout untreated passages at key timepoints coinciding with sequential antibiotic treatment.



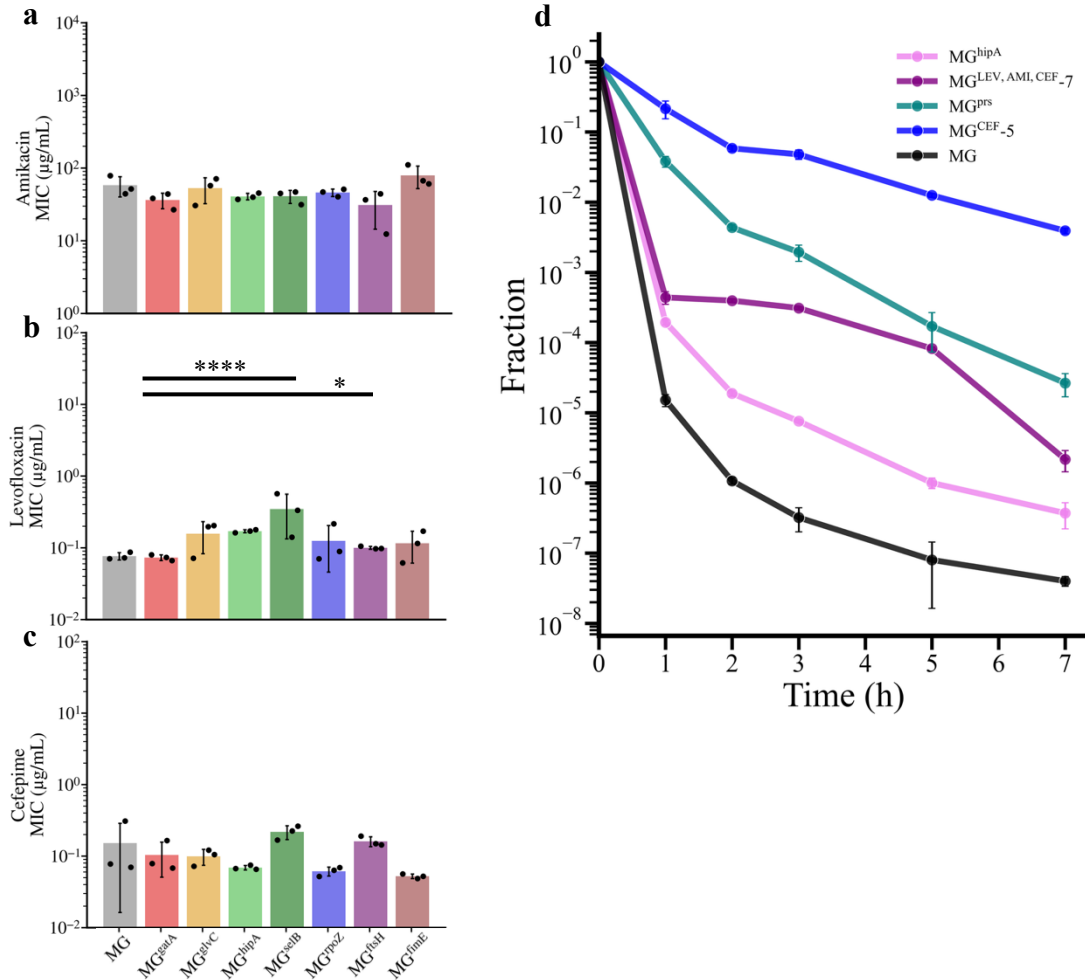
**Supplemental Figure 7. IC<sub>50</sub> and MIC values of sequentially evolved cultures.** a, Average IC<sub>50</sub> values (error bars: standard deviation) for individual cultures of parental strain (MG, gray) and cultures sequentially evolved in the presence of levofloxacin (MG<sup>LEV</sup>: red), then amikacin (MG<sup>LEV,AMI</sup>: blue), then cefepime (MG<sup>LEV,AMI,CEF</sup>: green), and b, Average MIC values (error bars: standard deviation) for individual cultures of parental strain (MG, gray) and cultures sequentially evolved in the presence of levofloxacin (MG<sup>LEV</sup>: red), then amikacin (MG<sup>LEV,AMI</sup>: blue), then cefepime (MG<sup>LEV,AMI,CEF</sup>: green).



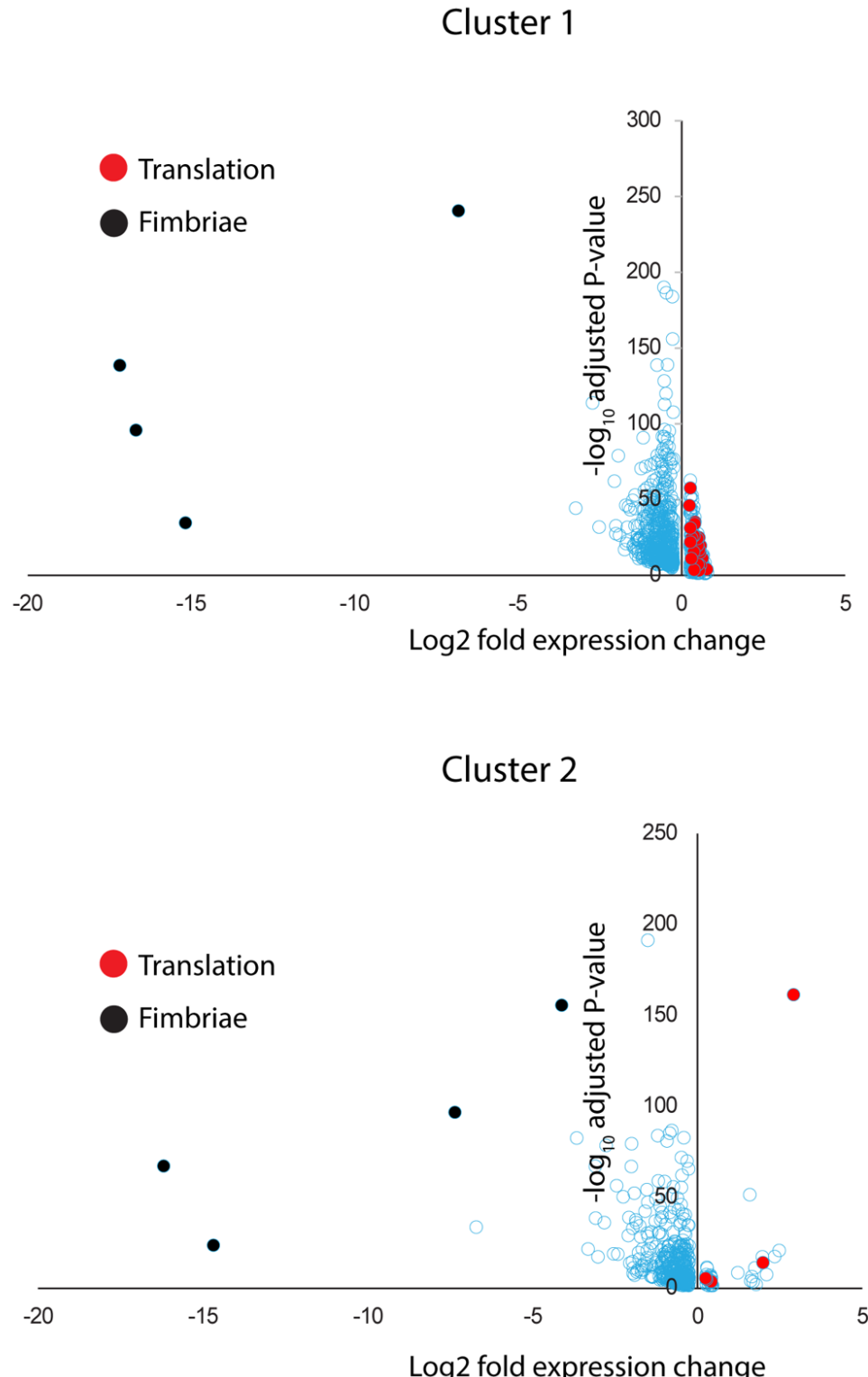
**Supplemental Figure 8. Selected mutation trajectories within each culture.** Emergence and fates of selected mutations throughout sequential antibiotic treatment. Columns a-e depict, respectively, mutations of *gyrA*, *rpoB*, *icd*, *fusA*, *trkH*, and those found to evolve convergently.



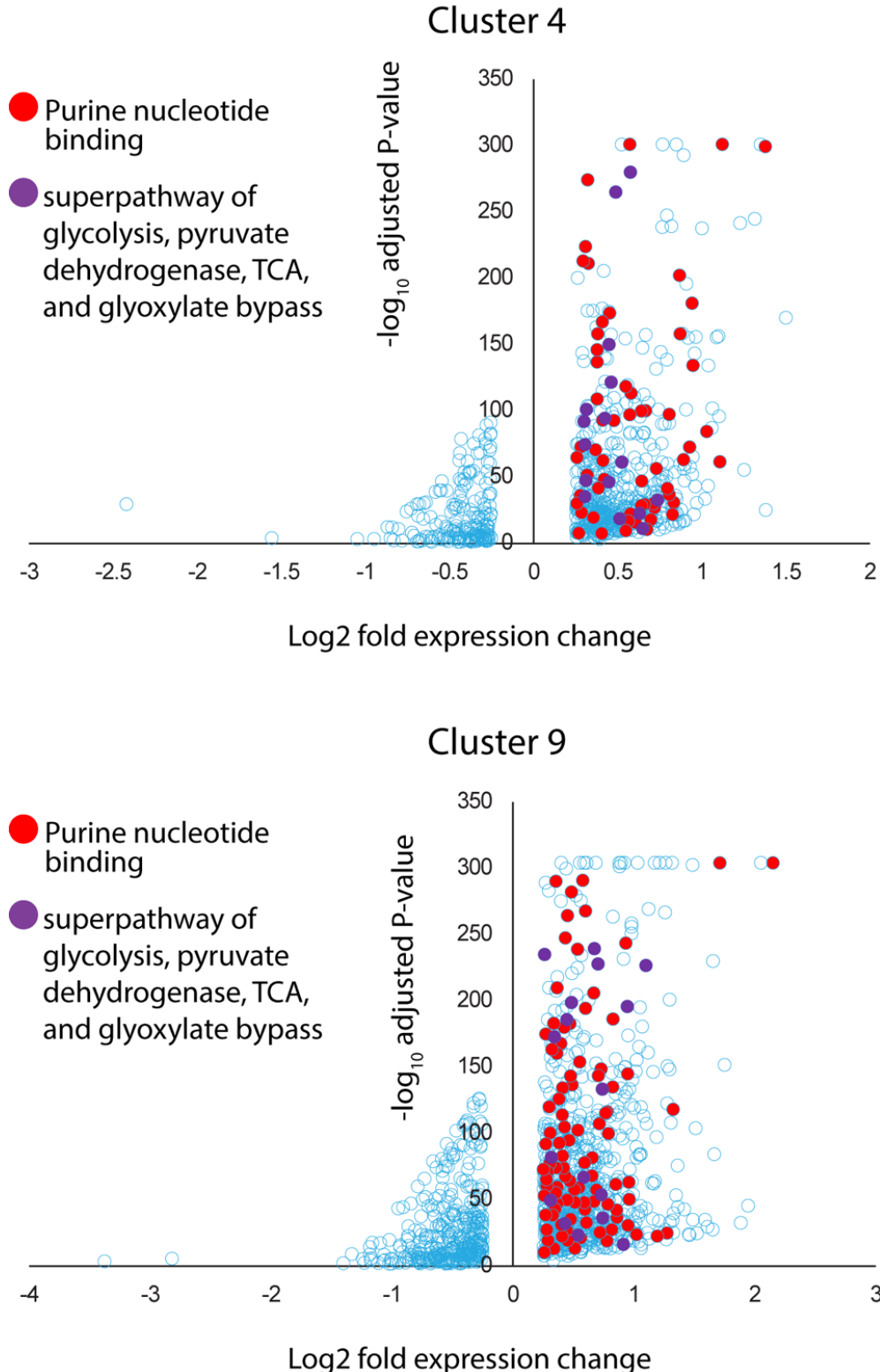
**Supplemental Figure 9. Comprehensive Mutation Frequency Heatmap.** All observed mutations among MG<sup>LEV</sup>, MG<sup>AMI</sup>, MG<sup>LEV,AMI</sup>, MG<sup>AMI,CEP</sup>, MG<sup>LEV,AMI,CEP</sup> cohorts (left to right) and their frequencies (color bar, right).



**Supplemental Figure 10. Extended individual mutation characterization.** a-c, MIC for individual mutants in each antibiotic, where bar height shows the mean value for three replicates (dots) and error bar indicates standard deviation. d, MDK of mutant strains and evolved cultures with median survival plotted for three replicates and error bar is the median absolute deviation.



**Supplemental Figure 11.** Volcano plots of genes differentially expressed in cluster 1 (top) and cluster 2 (bottom) compared to all other clusters in the combined dataset. Genes involved in protein translation that are overexpressed in these clusters are colored in red. Fimbriae related genes downregulated in these two clusters are colored black. For a full list of differentially regulated genes in each gene-set and P-values please refer to supplementary table 3.



**Supplemental Figure 12.** Volcano plots of genes differentially expressed in cluster 4 (top) and cluster 9 (bottom) compared to all other clusters in the combined dataset. Genes involved in purine nucleotide binding that are overexpressed in these clusters are colored in red. Genes in the superpathway of glycolysis, pyruvate dehydrogenase, TCA and Glyoxylate bypass that are overexpressed in these two clusters are colored in purple. For a full list of differentially regulated genes in each gene-set and P-values please refer to supplementary table 3.

Target Gene	Observed Mutation	Modification Made	Oligo nucleotide
<i>gata</i>	IS5 insertion within gene	added duplicate stop codons at insert site to truncate protein	ATGAACTTATTGTTGGCCTAA CAGATAAATGGCTGACGATTATTA CTTAGCATGAATGCCCTACAATG CGGTATTGCAATAGCGTG
<i>glvC</i>	1-nucleotide deletion	deleted nucleotide	CCATGTTGCCACCACACCAAAG AGATACATTACGGTCGACATTGGG CCGCCAGCACGGCGTGTACCGCA AACAGCAACGGTAAATGAA
<i>hipA</i>	SNP	alter nucleotide	TACGTGACCGGATCGTAAACGTT ATCATGCCAAATCCAGACAACTG TTTGTATTATTGTCAGAAATAGGG CGAGACAGCGTTGGTGC
<i>selB</i>	2-nucleotide insertion	insert nucleotides	CACCA CGG TCGT CACCA AACAG TGGCTCTGCTTTGCCAGATGTG GCCTGCTGCTTCGCTGAAGCC CGCTTGATCTGGCAGAT
<i>rpoZ</i>	7-nucleotide deletion	delete nucleotides	ACGCTGTAGAGAAAATTGGTAAC CGTTTGACCTGGTACTGGTCGTC GCGCTCGTCAGATGCAGGTAGGC GGAAAGGATCCGCTGGTACC
<i>ftsH</i>	12-nucleotide deletion	delete nucleotides	CAGCATCTGGTTCAAGATCTGTT ACGTTCATCGT GACCACCGCCAC GCTGGCGGCCTACGGCGTCGATT TCATCGATAAAGATGATGCA
<i>fimE</i>	IS5 insertion between promoter and transcription start	full gene deletion	AAC TTT ATTATCAATAAGTTAAC AATGATCCTGACGACGGAGACCG CCGTCGTCGACAAGCCCACAATA GTAGTACTCCTAACTGAGA

**Supplementary Table 1. Oligonucleotides for recobineering of individual mutants.** Detail of target genes, the mutations observed in each, the approach for modification, and the oligonucleotide used in transformation.

Gene	Primer Name	Full-length, Mutant-Specific, Both	Primer Direction	Sequence
<i>glvC</i>	fwd_glvC_full	Both	FWD	CATCTGCAAGAGTTCAGTTG
<i>glvC</i>	glvC_mt_rev	Mutant-Specific	REV	ACATTACGGTCGACATTGG
<i>glvC</i>	rev_glvC_full	Full-Length	REV	AGTAGAGTTTCACTTCCGCATC
<i>gatA</i>	fwd_gatA_full	Full-Length	FWD	AGGACGGTATATGACTAACCTG
<i>gatA</i>	fwd_gatA_stops	Mutant-Specific	FWD	GAGGCATTATCATGCTAAGTAAT
<i>gatA</i>	rev_gatA_full	Both	REV	GCAAGCGACAATAATCTTG
<i>selB</i>	fwd_selB_full	Full-Length	FWD	GTTATAGCTTGTGAATGCG
<i>selB</i>	fwd_selB_mut	Mutant-Specific	FWD	AGAGCAGCAGGCCACA
<i>selB</i>	rev_selB_full	Both	REV	GTTGAACCACACTCCTGAT
<i>hipA</i>	fwd_hipA_full	Full-Length	FWD	TCACTTGGATGAACAAACCAG
<i>hipA</i>	hipA_mt_fwd	Mutant-Specific	FWD	ATGCCAAATCCAGACAACT
<i>hipA</i>	rev_hipA_full	Both	REV	TTTAATGATGTGCGTCGTC
<i>rpoZ</i>	fwd_rpoZ_full	Full-Length	FWD	GAATGATGACTTCGATACCG
<i>rpoZ</i>	fwd_rpoZ_span	Mutant-Specific	FWD	TACTGGTCGTCGCGCT
<i>rpoZ</i>	rev_rpoZ_full	Both	REV	GACGCTTGATTGGTCTTC
<i>ftsH</i>	fwd_ftsH_full	Both	FWD	CAGAAACTCGGCGGTAAG
<i>ftsH</i>	rev_ftsH_full	Full-Length	REV	ATGTGAACCTTCAGGATCTGC
<i>ftsH</i>	rev_ftsHm_del	Mutant-Specific	REV	GACCACGCCACGCT
<i>fimE</i>	fwd_fimE_full	Full-Length	FWD	GACTGATAGCCACATCACTC
<i>fimE</i>	rev_fimE_del	Both	REV	CGTGCTTCCTCTATGAGTC
p57	pDel_seq_chlor_fwd	Mutant-Specific	FWD	GCGTTACATCCCTGGCTTGTG

**Supplementary Table 2. PCR Primers used for screening and confirming oligorecombineering mutations.**  
 Details of target PCR products, primer names, product type, primer direction, and sequence.

Sample name	Cell numbers
MG-3 replicate 1	7827
MG-3 replicate 2	10774
MG <sup>LEV,AMI,CEF</sup> -4 replicate 1	4764
MG <sup>LEV,AMI,CEF</sup> -4 replicate 2	2764
MG <sup>LEV,AMI,CEF</sup> -7 replicate 1	9619
MG <sup>LEV,AMI,CEF</sup> -7 replicate 2	13135
TOTAL CELLS	48883

Cluster name	Cell numbers
1	9335
2	7034
3	6008
4	5989
5	5092
6	4967
7	4961
8	3052
9	2445
TOTAL CELLS	48883

**Supplementary Table 3. scRNA sequencing samples statistics.** Samples (top) and clusters (bottom) and the number of cells representing each group.

## **References**

1. O'Neill, J. (2016). Tackling drug-resistant infections globally: final report and recommendations. *Review on Antimicrobial Resistance*.
2. Naghavi, M., Vollset, S., Ikuta, K., Swetschinski, L., Gray, A., Wool, E., and Aguilar, G. (2024). Global burden of bacterial antimicrobial resistance 1990-2021: a systematic analysis with forecasts to 2050. *Lancet* *404*, 1199-1226. 10.1016/s0140-6736(24)01867-1.
3. Park, K.H., Jung, Y.J., Lee, H.J., Kim, H.J., Maeng, C.H., Baek, S.K., Han, J.J., Jeon, W., Kim, D.Y., Lee, Y.M., and Lee, M.S. (2024). Impact of multidrug resistance on outcomes in hematologic cancer patients with bacterial bloodstream infections. *Scientific Reports* *14*, 15622. 10.1038/s41598-024-66524-w.
4. Ronneau, S., Hill, P.W., and Helaine, S. (2021). Antibiotic persistence and tolerance: not just one and the same. *Current opinion in microbiology* *64*, 76-81. 10.1016/j.mib.2021.09.017.
5. Rodrigues, M., Sabaeifard, P., Yildiz, M.S., Lyon, A., Coughlin, L., Ahmed, S., Poulides, N., Toprak, A.C., Behrendt, C., Wang, X., et al. (2024). Susceptible bacteria can survive antibiotic treatment in the mammalian gastrointestinal tract without evolving resistance. *Cell Host Microbe* *32*, 396-410.e396. 10.1016/j.chom.2024.01.012.
6. Bognár, B., Spohn, R., and Lázár, V. (2024). Drug combinations targeting antibiotic resistance. *npj Antimicrobials and Resistance* *2*, 29. 10.1038/s44259-024-00047-2.
7. Oz, T., Guvenek, A., Yildiz, S., Karaboga, E., Tamer, Y.T., Mumcuyan, N., Ozan, V.B., Senturk, G.H., Cokol, M., Yeh, P., and Toprak, E. (2014). Strength of selection pressure is an important parameter contributing to the complexity of antibiotic resistance evolution. *Molecular biology and evolution* *31*, 2387-2401. 10.1093/molbev/msu191.
8. Imamovic, L., and Sommer, M.O. (2013). Use of collateral sensitivity networks to design drug cycling protocols that avoid resistance development. *Sci Transl Med* *5*, 204ra132. 10.1126/scitranslmed.3006609.
9. Lazar, V., Pal Singh, G., Spohn, R., Nagy, I., Horvath, B., Hryyan, M., Busa-Fekete, R., Bogos, B., Mehi, O., Csorgo, B., et al. (2013). Bacterial evolution of antibiotic hypersensitivity. *Mol Syst Biol* *9*, 700.
10. Szybalski, W., and Bryson, V. (1952). Genetic studies on microbial cross resistance to toxic agents. I. Cross resistance of *Escherichia coli* to fifteen antibiotics. *J Bacteriol* *64*, 489-499.
11. Kim, S., Lieberman, T.D., and Kishony, R. (2014). Alternating antibiotic treatments constrain evolutionary paths to multidrug resistance. *Proc Natl Acad Sci U S A* *111*, 14494-14499. 10.1073/pnas.1409800111.
12. Kherroubi, L., Bacon, J., and Rahman, K.M. (2024). Navigating fluoroquinolone resistance in Gram-negative bacteria: a comprehensive evaluation. *JAC Antimicrob Resist* *6*, dlae127. 10.1093/jacamr/dlae127.

13. Serio, A.W., Keepers, T., Andrews, L., and Krause, K.M. (2018). Aminoglycoside Revival: Review of a Historically Important Class of Antimicrobials Undergoing Rejuvenation. *EcoSal Plus* 8. 10.1128/ecosalplus.ESP-0002-2018.
14. Rosenberg, C.R., Fang, X., and Allison, K.R. (2020). Potentiating aminoglycoside antibiotics to reduce their toxic side effects. *PLoS One* 15, e0237948. 10.1371/journal.pone.0237948.
15. Bush, K., and Bradford, P.A. (2016).  $\beta$ -Lactams and  $\beta$ -Lactamase Inhibitors: An Overview. *Cold Spring Harb Perspect Med* 6. 10.1101/cshperspect.a025247.
16. Eyler, R.F., and Shvets, K. (2019). Clinical Pharmacology of Antibiotics. *Clin J Am Soc Nephrol* 14, 1080-1090. 10.2215/cjn.08140718.
17. Munck, C., Gumpert, H.K., Wallin, A.I., Wang, H.H., and Sommer, M.O. (2014). Prediction of resistance development against drug combinations by collateral responses to component drugs. *Sci Transl Med* 6, 262ra156. 10.1126/scitranslmed.3009940.
18. Harmand, N., Gallet, R., Martin, G., and Lenormand, T. (2018). Evolution of bacteria specialization along an antibiotic dose gradient. *Evol Lett* 2, 221-232. 10.1002/evl3.52.
19. Monogue, M.L., and Nicolau, D.P. (2018). Antibacterial activity of ceftolozane/tazobactam alone and in combination with other antimicrobial agents against MDR *Pseudomonas aeruginosa*. *J Antimicrob Chemother* 73, 942-952. 10.1093/jac/dkx483.
20. Kiser, T.H., Hoody, D.W., Obritsch, M.D., Wegzyn, C.O., Bauling, P.C., and Fish, D.N. (2006). Levofloxacin pharmacokinetics and pharmacodynamics in patients with severe burn injury. *Antimicrob Agents Chemother* 50, 1937-1945. 10.1128/aac.01466-05.
21. Cao, G., Zhang, J., Wu, X., Yu, J., Chen, Y., Ye, X., Zhu, D., Zhang, Y., Guo, B., and Shi, Y. (2013). Pharmacokinetics and pharmacodynamics of levofloxacin injection in healthy Chinese volunteers and dosing regimen optimization. *J Clin Pharm Ther* 38, 394-400. 10.1111/jcpt.12074.
22. Windels, E.M., Fox, R., Yerramsetty, K., Krouse, K., Wenseleers, T., Swinnen, J., Matthay, P., Verstraete, L., Wilmaerts, D., Van den Bergh, B., and Michiels, J. (2021). Population Bottlenecks Strongly Affect the Evolutionary Dynamics of Antibiotic Persistence. *Molecular biology and evolution* 38, 3345-3357. 10.1093/molbev/msab107.
23. Mahrt, N., Tietze, A., Künzel, S., Franzenburg, S., Barbosa, C., Jansen, G., and Schulenburg, H. (2021). Bottleneck size and selection level reproducibly impact evolution of antibiotic resistance. *Nat Ecol Evol* 5, 1233-1242. 10.1038/s41559-021-01511-2.
24. Soothill, J.S., Ward, R., and Girling, A.J. (1992). The IC50: an exactly defined measure of antibiotic sensitivity. *J Antimicrob Chemother* 29, 137-139. 10.1093/jac/29.2.137.
25. Brauner, A., Fridman, O., Gefen, O., and Balaban, N.Q. (2016). Distinguishing between resistance, tolerance and persistence to antibiotic treatment. *Nat Rev Microbiol* 14, 320-330. 10.1038/nrmicro.2016.34.

26. Moyed, H.S., and Bertrand, K.P. (1983). *hipA*, a newly recognized gene of *Escherichia coli* K-12 that affects frequency of persistence after inhibition of murein synthesis. *J Bacteriol* *155*, 768-775. 10.1128/jb.155.2.768-775.1983.
27. Park, J., Lee, D., Yi, H., Yun, C.W., and Kim, H.S. (2024). Bacterial persistence to antibiotics activated by tRNA mutations. *J Antimicrob Chemother* *79*, 2923-2931. 10.1093/jac/dkae307.
28. Van den Bergh, B., Schramke, H., Michiels, J.E., Kimkes, T.E.P., Radzikowski, J.L., Schimpf, J., Vedelaar, S.R., Burschel, S., Dewachter, L., Lončar, N., et al. (2022). Mutations in respiratory complex I promote antibiotic persistence through alterations in intracellular acidity and protein synthesis. *Nat Commun* *13*, 546. 10.1038/s41467-022-28141-x.
29. Liakopoulos, A., Aulin, L.B.S., Buffoni, M., Fragkiskou, E., van Hasselt, J.G.C., and Rozen, D.E. (2022). Allele-specific collateral and fitness effects determine the dynamics of fluoroquinolone resistance evolution. *Proc Natl Acad Sci U S A* *119*, e2121768119. 10.1073/pnas.2121768119.
30. Yoshida, H., Bogaki, M., Nakamura, M., and Nakamura, S. (1990). Quinolone resistance-determining region in the DNA gyrase *gyrA* gene of *Escherichia coli*. *Antimicrob Agents Chemother* *34*, 1271-1272. 10.1128/aac.34.6.1271.
31. Nandy, P., Chib, S., and Seshasayee, A. (2020). A Mutant RNA Polymerase Activates the General Stress Response, Enabling *Escherichia coli* Adaptation to Late Prolonged Stationary Phase. *mSphere* *5*. 10.1128/mSphere.00092-20.
32. Fraebel, D.T., Mickalide, H., Schnitkey, D., Merritt, J., Kuhlman, T.E., and Kuehn, S. (2017). Environment determines evolutionary trajectory in a constrained phenotypic space. *eLife* *6*. 10.7554/eLife.24669.
33. Boël, G., Letso, R., Neely, H., Price, W.N., Wong, K.H., Su, M., Luff, J., Valecha, M., Everett, J.K., Acton, T.B., et al. (2016). Codon influence on protein expression in *E. coli* correlates with mRNA levels. *Nature* *529*, 358-363. 10.1038/nature16509.
34. Pietsch, F., Bergman, J.M., Brandis, G., Marcusson, L.L., Zorzet, A., Huseby, D.L., and Hughes, D. (2017). Ciprofloxacin selects for RNA polymerase mutations with pleiotropic antibiotic resistance effects. *J Antimicrob Chemother* *72*, 75-84. 10.1093/jac/dkw364.
35. Fridman, O., Goldberg, A., Ronin, I., Shores, N., and Balaban, N.Q. (2014). Optimization of lag time underlies antibiotic tolerance in evolved bacterial populations. *Nature* *513*, 418-421. 10.1038/nature13469.
36. Adler, M., Anjum, M., Andersson, D.I., and Sandegren, L. (2016). Combinations of mutations in *envZ*, *ftsI*, *mrdA*, *acrB* and *acrR* can cause high-level carbapenem resistance in *Escherichia coli*. *J Antimicrob Chemother* *71*, 1188-1198. 10.1093/jac/dkv475.
37. Gerken, H., Shetty, D., Kern, B., Kenney, L.J., and Misra, R. (2024). Effects of pleiotropic *ompR* and *envZ* alleles of *Escherichia coli* on envelope stress and antibiotic sensitivity. *J Bacteriol* *206*, e0017224. 10.1128/jb.00172-24.

38. Zhou, G., Wang, Q., Wang, Y., Wen, X., Peng, H., Peng, R., Shi, Q., Xie, X., and Li, L. (2023). Outer Membrane Porins Contribute to Antimicrobial Resistance in Gram-Negative Bacteria. *Microorganisms* *11*. 10.3390/microorganisms11071690.
39. Ma, D., Alberti, M., Lynch, C., Nikaido, H., and Hearst, J.E. (1996). The local repressor AcrR plays a modulating role in the regulation of acrAB genes of *Escherichia coli* by global stress signals. *Mol Microbiol* *19*, 101-112. 10.1046/j.1365-2958.1996.357881.x.
40. Cohen, S.P., Hächler, H., and Levy, S.B. (1993). Genetic and functional analysis of the multiple antibiotic resistance (mar) locus in *Escherichia coli*. *J Bacteriol* *175*, 1484-1492. 10.1128/jb.175.5.1484-1492.1993.
41. Okusu, H., Ma, D., and Nikaido, H. (1996). AcrAB efflux pump plays a major role in the antibiotic resistance phenotype of *Escherichia coli* multiple-antibiotic-resistance (Mar) mutants. *J Bacteriol* *178*, 306-308. 10.1128/jb.178.1.306-308.1996.
42. Reizer, J., Michotey, V., Reizer, A., and Saier, M.H., Jr. (1994). Novel phosphotransferase system genes revealed by bacterial genome analysis: unique, putative fructose- and glucoside-specific systems. *Protein Sci* *3*, 440-450. 10.1002/pro.5560030309.
43. Homma, K., Fukuchi, S., Kawabata, T., Ota, M., and Nishikawa, K. (2002). A systematic investigation identifies a significant number of probable pseudogenes in the *Escherichia coli* genome. *Gene* *294*, 25-33. 10.1016/s0378-1119(02)00794-1.
44. Forchhammer, K., Leinfelder, W., and Böck, A. (1989). Identification of a novel translation factor necessary for the incorporation of selenocysteine into protein. *Nature* *342*, 453-456. 10.1038/342453a0.
45. Abraham, J.M., Freitag, C.S., Clements, J.R., and Eisenstein, B.I. (1985). An invertible element of DNA controls phase variation of type 1 fimbriae of *Escherichia coli*. *Proc Natl Acad Sci U S A* *82*, 5724-5727. 10.1073/pnas.82.17.5724.
46. Stentebjerg-Olesen, B., Chakraborty, T., and Klemm, P. (2000). FimE-catalyzed off-to-on inversion of the type 1 fimbrial phase switch and insertion sequence recruitment in an *Escherichia coli* K-12 fimB strain. *FEMS Microbiol Lett* *182*, 319-325. 10.1111/j.1574-6968.2000.tb08915.x.
47. Tomoyasu, T., Gamer, J., Bukau, B., Kanemori, M., Mori, H., Rutman, A.J., Oppenheim, A.B., Yura, T., Yamanaka, K., Niki, H., and et al. (1995). *Escherichia coli* FtsH is a membrane-bound, ATP-dependent protease which degrades the heat-shock transcription factor sigma 32. *Embo j* *14*, 2551-2560. 10.1002/j.1460-2075.1995.tb07253.x.
48. Griffith, K.L., Shah, I.M., and Wolf, R.E., Jr. (2004). Proteolytic degradation of *Escherichia coli* transcription activators SoxS and MarA as the mechanism for reversing the induction of the superoxide (SoxRS) and multiple antibiotic resistance (Mar) regulons. *Mol Microbiol* *51*, 1801-1816. 10.1046/j.1365-2958.2003.03952.x.

49. Volpon, L., Young, C.R., Matte, A., and Gehring, K. (2006). NMR structure of the enzyme GatB of the galactitol-specific phosphoenolpyruvate-dependent phosphotransferase system and its interaction with GatA. *Protein Sci* *15*, 2435-2441. 10.1110/ps.062337406.
50. Yang, J., Peng, Z., Ji, X., Zhang, J., and Du, G. (2022). Galactitol Transport Factor GatA Relieves ATP Supply Restriction to Enhance Acid Tolerance of *Escherichia coli* in the Two-Stage Fermentation Production of D-Lactate. *Fermentation* *8*.
51. Saunders, S.H., and Ahmed, A.M. (2024). ORBIT for *E. coli*: kilobase-scale oligonucleotide recombineering at high throughput and high efficiency. *Nucleic Acids Research* *52*, e43-e43. 10.1093/nar/gkae227.
52. Gilbert, P., Collier, P.J., and Brown, M.R. (1990). Influence of growth rate on susceptibility to antimicrobial agents: biofilms, cell cycle, dormancy, and stringent response. *Antimicrobial Agents and Chemotherapy* *34*, 1865-1868. doi:10.1128/aac.34.10.1865.
53. McNulty, R., Sritharan, D., Pahng, S.H., Meisch, J.P., Liu, S., Brennan, M.A., Saxon, G., Hormoz, S., and Rosenthal, A.Z. (2023). Probe-based bacterial single-cell RNA sequencing predicts toxin regulation. *Nature Microbiology* *8*, 934-945. 10.1038/s41564-023-01348-4.
54. Wood, W.N., Mohler, K., Rinehart, J., and Ibba, M. (2021). Deacylated tRNA Accumulation Is a Trigger for Bacterial Antibiotic Persistence Independent of the Stringent Response. *mBio* *12*, 10.1128/mbio.01132-01121. doi:10.1128/mbio.01132-21.
55. Toprak, E., Veres, A., Michel, J.B., Chait, R., Hartl, D.L., and Kishony, R. (2011). Evolutionary paths to antibiotic resistance under dynamically sustained drug selection. *Nat Genet* *44*, 101-105. 10.1038/ng.1034.
56. Lopatkin, A.J., Bening, S.C., Manson, A.L., Stokes, J.M., Kohanski, M.A., Badran, A.H., Earl, A.M., Cheney, N.J., Yang, J.H., and Collins, J.J. (2021). Clinically relevant mutations in core metabolic genes confer antibiotic resistance. *Science* *371*. 10.1126/science.aba0862.
57. Sørum, V., Øynes, E.L., Møller, A.S., Harms, K., Samuelsen, Ø., Podneicky, N.L., and Johnsen, P.J. (2022). Evolutionary Instability of Collateral Susceptibility Networks in Ciprofloxacin-Resistant Clinical *Escherichia coli* Strains. *mBio* *13*, e0044122. 10.1128/mbio.00441-22.
58. Barbosa, C., Römhild, R., Rosenstiel, P., and Schulenburg, H. (2019). Evolutionary stability of collateral sensitivity to antibiotics in the model pathogen *Pseudomonas aeruginosa*. *eLife* *8*. 10.7554/eLife.51481.
59. Avershina, E., Khezri, A., and Ahmad, R. (2023). Clinical Diagnostics of Bacterial Infections and Their Resistance to Antibiotics-Current State and Whole Genome Sequencing Implementation Perspectives. *Antibiotics (Basel)* *12*. 10.3390/antibiotics12040781.
60. Friedman, S.M., Lu, T., and Drlica, K. (2001). Mutation in the DNA gyrase A Gene of *Escherichia coli* that expands the quinolone resistance-determining region. *Antimicrob Agents Chemother* *45*, 2378-2380. 10.1128/aac.45.8.2378-2380.2001.

61. Barrett, R.D., and Schluter, D. (2008). Adaptation from standing genetic variation. *Trends Ecol Evol* 23, 38-44. 10.1016/j.tree.2007.09.008.
62. Diaz Caballero, J., Wheatley, R.M., Kapel, N., López-Causapé, C., Van der Schalk, T., Quinn, A., Shaw, L.P., Ogunlana, L., Recanatini, C., Xavier, B.B., et al. (2023). Mixed strain pathogen populations accelerate the evolution of antibiotic resistance in patients. *Nat Commun* 14, 4083. 10.1038/s41467-023-39416-2.
63. Korch, S.B., Henderson, T.A., and Hill, T.M. (2003). Characterization of the hipA7 allele of *Escherichia coli* and evidence that high persistence is governed by (p)ppGpp synthesis. *Mol Microbiol* 50, 1199-1213. 10.1046/j.1365-2958.2003.03779.x.
64. Germain, E., Castro-Roa, D., Zenkin, N., and Gerdes, K. (2013). Molecular mechanism of bacterial persistence by HipA. *Mol Cell* 52, 248-254. 10.1016/j.molcel.2013.08.045.
65. Kaspy, I., Rotem, E., Weiss, N., Ronin, I., Balaban, N.Q., and Glaser, G. (2013). HipA-mediated antibiotic persistence via phosphorylation of the glutamyl-tRNA-synthetase. *Nat Commun* 4, 3001. 10.1038/ncomms4001.
66. Schumacher, M.A., Balani, P., Min, J., Chinnam, N.B., Hansen, S., Vulić, M., Lewis, K., and Brennan, R.G. (2015). HipBA-promoter structures reveal the basis of heritable multidrug tolerance. *Nature* 524, 59-64. 10.1038/nature14662.
67. Semanjski, M., Germain, E., Bratl, K., Kiessling, A., Gerdes, K., and Macek, B. (2018). The kinases HipA and HipA7 phosphorylate different substrate pools in *Escherichia coli* to promote multidrug tolerance. *Sci Signal* 11. 10.1126/scisignal.aat5750.
68. Yu, H., and Kim, K.S. (2011). The involvement of SelB in the expression of cytotoxic necrotizing factor 1 in *Escherichia coli*. *FEBS Lett* 585, 1934-1940. 10.1016/j.febslet.2011.05.012.
69. Kwan, B.W., Valenta, J.A., Benedik, M.J., and Wood, T.K. (2013). Arrested protein synthesis increases persister-like cell formation. *Antimicrob Agents Chemother* 57, 1468-1473. 10.1128/aac.02135-12.
70. Lane, M.C., Simms, A.N., and Mobley, H.L. (2007). complex interplay between type 1 fimbrial expression and flagellum-mediated motility of uropathogenic *Escherichia coli*. *J Bacteriol* 189, 5523-5533. 10.1128/jb.00434-07.
71. Narberhaus, F., Obrist, M., Führer, F., and Langklotz, S. (2009). Degradation of cytoplasmic substrates by FtsH, a membrane-anchored protease with many talents. *Res Microbiol* 160, 652-659. 10.1016/j.resmic.2009.08.011.
72. Schäkermann, M., Langklotz, S., and Narberhaus, F. (2013). FtsH-mediated coordination of lipopolysaccharide biosynthesis in *Escherichia coli* correlates with the growth rate and the alarmone (p)ppGpp. *J Bacteriol* 195, 1912-1919. 10.1128/jb.02134-12.

73. Langklotz, S., Baumann, U., and Narberhaus, F. (2012). Structure and function of the bacterial AAA protease FtsH. *Biochim Biophys Acta* *1823*, 40-48. 10.1016/j.bbamcr.2011.08.015.
74. Zuo, Y., Wang, Y., and Steitz, T.A. (2013). The mechanism of *E. coli* RNA polymerase regulation by ppGpp is suggested by the structure of their complex. *Mol Cell* *50*, 430-436. 10.1016/j.molcel.2013.03.020.
75. Ross, W., Sanchez-Vazquez, P., Chen, A.Y., Lee, J.H., Burgos, H.L., and Gourse, R.L. (2016). ppGpp Binding to a Site at the RNAP-DksA Interface Accounts for Its Dramatic Effects on Transcription Initiation during the Stringent Response. *Mol Cell* *62*, 811-823. 10.1016/j.molcel.2016.04.029.
76. Deatherage, D.E., and Barrick, J.E. (2014). Identification of mutations in laboratory-evolved microbes from next-generation sequencing data using breseq. *Methods in molecular biology* *1151*, 165-188. 10.1007/978-1-4939-0554-6\_12.
77. Nyerges, Á., Csörgő, B., Nagy, I., Bálint, B., Bihari, P., Lázár, V., Apjok, G., Umenhoffer, K., Bogos, B., Pósfaí, G., and Pál, C. (2016). A highly precise and portable genome engineering method allows comparison of mutational effects across bacterial species. *Proc Natl Acad Sci U S A* *113*, 2502-2507. 10.1073/pnas.1520040113.
78. Samanta, P., Cooke, S.F., McNulty, R., Hormoz, S., and Rosenthal, A. (2024). ProBac-seq, a bacterial single-cell RNA sequencing methodology using droplet microfluidics and large oligonucleotide probe sets. *Nature protocols* *19*, 2939-2966. 10.1038/s41596-024-01002-1.
79. McNulty, R., Sritharan, D., Pahng, S.H., Meisch, J.P., Liu, S., Brennan, M.A., Saxer, G., Hormoz, S., and Rosenthal, A.Z. (2023). Probe-based bacterial single-cell RNA sequencing predicts toxin regulation. *Nat Microbiol* *8*, 934-945. 10.1038/s41564-023-01348-4.
80. Stuart, T., Butler, A., Hoffman, P., Hafemeister, C., Papalex, E., Mauck, W.M., 3rd, Hao, Y., Stoeckius, M., Smibert, P., and Satija, R. (2019). Comprehensive Integration of Single-Cell Data. *Cell* *177*, 1888-1902 e1821. 10.1016/j.cell.2019.05.031.